



Available online at www.sciencedirect.com

ScienceDirect

Geochimica et Cosmochimica Acta

Geochimica et Cosmochimica Acta 268 (2020) 422-445

www.elsevier.com/locate/gca

Sulfide mantle source heterogeneity recorded in basaltic lavas from the Azores

Christopher L. Waters a,b, James M.D. Day a,*, Shizuko Watanabe c,d, Kaan Sayit e,f, Vittorio Zanon g, Kristina M. Olson Barry B. Hanan e, Elisabeth Widom c

a Scripps Institution of Oceanography, University of California San Diego, La Jolla, CA 92093-0244, USA
b San Diego Mesa College, 7250 Mesa College Drive, San Diego, CA 92111-4998, USA
c Department of Geology and Environmental Earth Science, Miami University, Oxford, OH 45056, USA
d Department of Geology, Eastfield College, Mesquite, TX 75150, USA
c Department of Geological Sciences, San Diego State University, San Diego, CA 92182, USA
f Department of Geological Engineering, Middle East Technical University, 06800 Ankara, Turkey
Instituto de Investigação em Vulcanologia e Avaliação de Riscos, Universidade dos Açores, Rua Mãe de Deus, 9500-321 Ponta
Delgada, Portugal

Received 8 June 2019; accepted in revised form 7 October 2019; Available online 25 October 2019

Abstract

New highly siderophile element (HSE: Os, Ir, Ru, Pt, Pd, Re) abundance and Os isotopic compositions, along with major- and trace-element abundance and Sr-Nd-Hf-Pb isotope data are reported for high-MgO (>8–17 wt.%) lavas from the islands of São Miguel, Terceira, Pico and Faial in the Azores archipelago. The lavas span the range of Sr-Nd-Hf-Pb isotope and trace-element abundance variability reported previously for the islands. Pico and Faial lavas preserve distinct absolute and relative HSE abundances and 187 Os/ 188 Os ($\Sigma_{HSE} = 2 \pm 2$ ng g $^{-1}$; 2SD; 187 Os/ 188 Os in lavas with > 50 pg g $^{-1}$ Os = 0.1255 \pm 31; 2SD) compared with São Miguel and Terceira lavas ($\Sigma_{HSE} = 5 \pm 3$ ng g $^{-1}$; 187 Os/ 188 Os_{50pg} = 0.1284 \pm 48). Although HSE abundance variations in volcanic rocks from individual Azorean islands can be explained by sulfide crystallization, those between Pico and Faial and São Miguel and Terceira can only reasonably be attributed to partial melting of distinct mantle sources.

Pico and Faial lava compositions are consistent with high degrees of sulfide melting (90–100%) from a sulfide-depleted mantle source (<100 ppm) with relatively unradiogenic ¹⁸⁷Os/¹⁸⁸Os (<0.126). São Miguel and Terceira lavas likely derive from a sulfide-enriched (300–600 ppm) mantle source that underwent lesser degrees of sulfide melting (1–15%), with more radiogenic ¹⁸⁷Os/¹⁸⁸Os (>0.128). Radiogenic sulfides are not solely linked to the enriched lithophile isotope signature found in eastern São Miguel. Instead, São Miguel and Terceira magmatism may collectively result from metasomatism associated with the recycling of old subducted oceanic lithosphere. Abundances of sulfide-hosted HSE and ¹⁸⁷Os/¹⁸⁸Os are decoupled from silicate-hosted Sr-Nd-Hf-Pb isotope compositions in the mantle. Compositional variations of the HSE among global OIB suggest that, while distinct mantle domains are represented by heterogeneous sulfide mineralogy, comprising common metasomatic (enriched) and magmatic (depleted) compositions, these sulfide populations are distinct beneath different OIB due to their origin in different lithospheric materials (e.g., oceanic crust versus pelagic sediment), and to the degree of partial melting caused by variable mantle potential temperature or lithospheric thickness.

© 2019 Elsevier Ltd. All rights reserved.

Keywords: Osmium isotopes; Highly siderophile elements; Ocean island basalts; Sulfides; Mantle heterogeneity; Azores

E-mail address: jmdday@ucsd.edu (J.M.D. Day).

^{*} Corresponding author.

1. INTRODUCTION

Lithophile radiogenic isotope (Sr, Nd, Hf, Pb) and incompatible trace element studies of ocean island basalts (OIB) provide evidence for mantle heterogeneity and of widespread, compositionally diverse silicate mantle reservoirs (e.g., Gast et al., 1964; White and Hofmann, 1982; Zindler and Hart, 1986; Blichert-Toft and Albarède, 1997; Elliott et al., 2007). In contrast, there is limited evidence from partial melts for highly siderophile element (HSE: Os, Ir, Ru, Rh, Pt, Pd, Au, and Re) relative or absolute abundance heterogeneity in the present-day mantle (Ireland et al., 2009; Day et al., 2010; Day, 2013; Peters et al., 2016). This lack of heterogeneity in HSE abundances is perplexing given large variations in ¹⁸⁷Os/¹⁸⁸Os (0.124– 0.175) for OIB that reflect long-term parent-daughter Re/ Os variation within the mantle (e.g., Pegram and Allègre, 1992; Hauri and Hart, 1993; Reisberg et al., 1993; Widom and Shirey, 1996; Lassiter and Hauri, 1998; Brandon et al., 1999; Widom et al., 1999; Schiano et al., 2001; Eisele et al., 2002; Lassiter et al., 2003; Brandon et al., 2007; Class et al., 2009; Day et al., 2009, 2010; Ireland et al., 2009; Gibson et al., 2016; Paquet et al., 2019). Furthermore, experimental studies and detailed measurements of mineral phases in mantle peridotite show that sulfides, which dominate the HSE budget of the mantle, have variable compositions, HSE abundances, and 187Os/188Os (e.g., Alard et al., 2000, 2005; Luguet et al., 2001; Bockrath et al., 2004; Harvey et al., 2011; Lorand and Luguet, 2016). Interpretation of observed HSE heterogeneities is complicated by partial melting and crystalliquid fractionation processes that obscure mantle-derived HSE abundance fractionation (Day, 2013). Nonetheless, definitive identification of HSE abundance heterogeneities in mantle-derived volcanic rocks would offer new constraints on the composition of the convecting mantle.

Here we provide data for basalts from the Azores archipelago, which are characterized by significant radiogenic isotope heterogeneity, in order to investigate potential HSE mantle source differences. The Azores are located in the central North Atlantic Ocean between 37° and 40°N, at the North American, African, and Eurasian plate triple junction and comprise nine islands. These are predominantly composed of alkali olivine basalts and their cogenetic differentiates (White et al., 1979; Fig. 1). Previous studies of major and trace element abundances, and Sr-Nd-Hf-Pb isotope compositions have reported spatially correlated mixing trends between a MORB-like end member and a globally-unique, enriched end member among lavas from São Miguel island, characterized by high ²⁰⁸-Pb/²⁰⁴Pb and ²⁰⁷Pb/²⁰⁴Pb at relatively low ²⁰⁶Pb/²⁰⁴Pb, radiogenic ⁸⁷Sr/⁸⁶Sr, and unradiogenic ¹⁴³Nd/¹⁴⁴Nd and ¹⁷⁶Hf/¹⁷⁷Hf (White et al., 1979; Turner et al., 1997; Widom et al., 1997; Beier et al., 2007; Elliott et al., 2007; Genske et al., 2016).

By contrast, lavas from São Jorge, Terceira, Pico and Faial mark a trend linking a MORB-like end member, similar to that associated with the tholeiitic submarine Azores platform, towards an end-member characterized by high $^{206}\text{Pb/}^{204}\text{Pb}$ (Elliott et al., 2007; Beier et al., 2008; Millet et al., 2009). Ultimately, basalts from the Azores archipelago show inter- and intra-island lithophile element, and Sr-Nd-Hf-Pb isotopic heterogeneity, attributed to spatially heterogeneous mantle delivering a diverse range of recycled materials - including terrigenous sediments, metasomatized

subcontinental lithosphere, and mafic crust - to the melting region (Widom and Shirey, 1996; Turner et al., 1997; Widom et al., 1997; Schaefer et al., 2002; Beier et al., 2007, 2008; Elliott et al., 2007; Millet et al., 2009). Using samples from the islands of São Miguel, Pico, Faial, and Terceira that span the range of previously identified isotopic heterogeneity, we show that HSE abundances and ¹⁸⁷-Os/¹⁸⁸Os in Azorean lavas track heterogeneous mantle sulfide mineralogy, providing a complementary geochemical record of mantle source heterogeneity to lithophile incompatible trace elements, radiogenic isotopes (e.g., Sr, Nd, Pb, Hf), stable isotopes (e.g., B, Li, O; Widom and Farquhar, 2003; Genske et al., 2014), and noble gases (e.g., He, Ne; Madureira et al., 2005; Moreira et al., 1999).

2. SAMPLES AND METHODS

More than 40 samples collected from the islands of São Miguel, Pico, Faial, and Terceira during several sampling campaigns, and from the local Mid-Atlantic Ridge segment were investigated in this study (Table S1). These include remeasurement of samples from Pico (P5) and Faial (F/CA 6) that have been reported to have unusually low, subchondritic ¹⁸⁷Os/¹⁸⁸Os, and used to infer the presence of recycled Archaean continental lithosphere in the Azorean mantle source (Schaefer et al., 2002). We preferentially sampled lavas with high olivine and clinopyroxene modal abundances. High-MgO lavas typically originate from more primitive magmas, or are accumulative, and are generally less sensitive to the effects of crustal contamination, making them useful for HSE and Os isotope studies (Day, 2013). Additionally, two analyses are presented for a Mid-Atlantic Ridge (MAR) glass sample (AII-0127-D44-1) that were also examined by Genske et al. (2016).

Samples were prepared using a diamond-bladed tile saw to make centimeter-sized slabs, from which metallic saw marks were removed with 600-grit silicon carbide paper. The slabs were then crushed to mm-sized rock chips in an alumina ceramic mini-jaw crusher, and subsequently powdered in a shatter box using an alumina ceramic grinding container. Mineral modes and petrography (Table S1) were established using polished sections of samples. Distortion-free, scaled photo-mosaics (e.g., Fig. S1) were constructed and modes were determined by color and textural contrast, using *image J*, as described in Day et al. (2014). All mineral determinations were confirmed with a polarizing light microscope.

2.1. Whole-rock major and trace element abundances

Major element compositions were measured by X-ray fluorescence (XRF) at Franklin and Marshall College using a PW 2404 *PANalytical* XRF vacuum spectrometer following the procedures outlined in Boyd and Mertzman (1987). Precision is estimated using replicate analyses of standards, with long-term reproducibility (in wt.% and 2 σ absolute standard deviation, n=13) of ± 0.13 for SiO₂, ± 0.01 for TiO₂, ± 0.09 for Al₂O₃, ± 0.63 for FeO, ± 0.47 for Fe₂O₃, ± 0.10 for Fe₂O₃, ± 0.01 for MnO, ± 0.04 for MgO, ± 0.07 for CaO, ± 0.03 for Na₂O, ± 0.01 for K₂O, and $\pm < 0.01$ for P₂O₅. Accuracy for the average of 13 runs of BHVO-2 relative to USGS accepted values is better than 0.2% for SiO₂ and TiO₂, < 1% for Al₂O₃, MgO, Fe₂O₃^T, CaO, Na₂O, P₂O₅, and < 3% for K₂O.

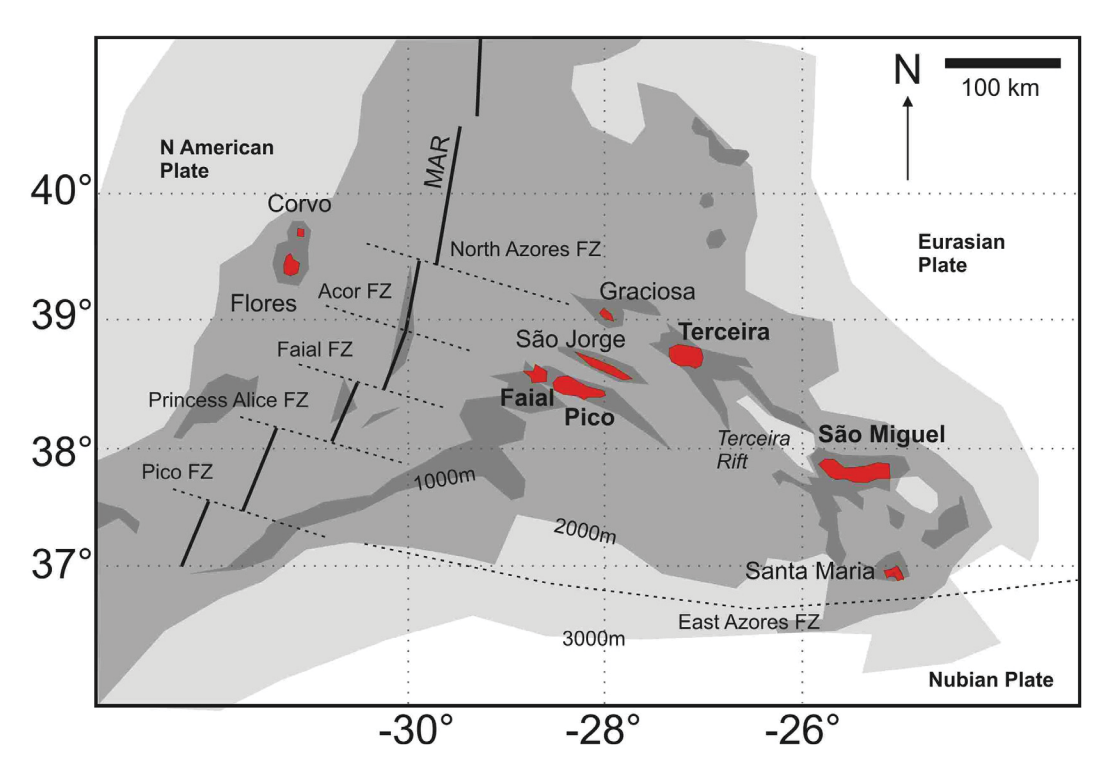


Fig. 1. Map of the Azores archipelago showing bathymetry and island locations (sampled islands in bold). Major features, including the Mid-Atlantic Ridge (MAR), Terceira Rift and fracture zones (FZ) are also indicated. X axis is in degrees longitude W, Y axis is in degrees latitude N.

Trace-element abundances were determined at the Scripps Isotope Geochemistry Laboratory (SIGL). Scripps Institution of Oceanography using methods described in Day et al., (2014). One hundred milligrams of rock powder was precisely weighed and digested in a 1:4 mixture of Teflon-distilled HNO₃:HF for >72 h at 150 °C on a hotplate. Rock standards (BHVO-2, BIR-1, BCR-2, AGV-2, GP13. DTS-2b) and total procedural blanks were prepared along with the samples. After drying down, and sequential HNO₃ dry-down steps to break-down fluorides, clear sample solutions were diluted by a factor of 5000 in 2% HNO₃ and doped with a 1 ppb In solution to monitor instrumental drift. Solutions were measured using a Thermo Scientific iCAPOc quadrupole inductively coupled plasma mass spectrometer at the SIGL in standard mode. Reproducibility of the reference materials was generally better than 5% (RSD) for basaltic and peridotite standards, and element abundances were generally within error (1 SD) of recommended values. Data for standard powders run as unknowns with samples as well as the entire dataset are provided in the supplementary tables accompanying this manuscript.

2.2. Strontium-Nd-Hf-Pb isotope analyses

Strontium, Nd, Pb and Hf were purified from powders and analyzed at San Diego State University (SDSU; Nd, Hf, Pb) and at the *SIGL* (Sr) using methods most recently outlined by Rooney et al. (2012), and previously detailed by Hanan and Schilling (1989). Neodymium and Hf isotopes were measured on a *Nu Plasma HR* multi-collector inductively coupled plasma mass spectrometer (MC-ICP-MS) and Pb isotope compositions were measured on a *Nu*

1700 MC-ICP-MS, with both instruments interfaced using a *Nu instruments* desolvating nebulizer equipped with a 100 μ l/min nebulizer (DSN100). Strontium isotope ratios were measured on the *ThermoScientific* Triton thermal ionization mass spectrometer at the *SIGL*, with data normalized to ⁸⁶Sr/⁸⁸Sr = 0.1194 to correct for mass fractionation and reported relative to NIST SRM 987 = 0.710250. 300 ng loads of the NBS 987 Sr standard gave an average ⁸⁷Sr/⁸⁶Sr value of 0.710233 \pm 5 (2SE [sigma error]; n = 7). Three separate digestions of the BHVO-2 standard gave 0.703458 \pm 2, which is within uncertainty of the suggested value from GEOREM of 0.703469 \pm 17.

The Nd and Hf isotope ratios were corrected for instrumental mass fractionation and machine bias by applying a discrimination factor determined by bracketing sample runs with analyses of the SDSU AMES Nd and the JMC 475 standards (every two to three samples). Hafnium isotope sample data were normalized to $^{179}\mathrm{Hf}/^{177}\mathrm{Hf} = 0.7325$ and are reported relative to JMC 475 = 0.282162. External uncertainties were 9 ppm (2SE) on JMC 475 measurements during the analytical campaign. Neodymium isotope sample data were normalized to $^{146}\mathrm{Nd}/^{144}\mathrm{Nd} = 0.7219$ and are reported relative to the lab value of $^{143}\mathrm{Nd}/^{144}\mathrm{Nd} = 0.512130$ for the SDSU AMES Nd standard. The measured values of the La Jolla standards at SDSU during the campaign was 0.511844 ± 4 (2SE).

For Pb, instrumental mass bias was monitored and corrected using the NIST SRM 997 Tl internal standard (205 -Tl/ 203 Tl = 2.3889) and bracketing standard NIST SRM 981 (run every 1–2 samples), assuming values of 208 Pb/ 204 -Pb = 36.7006, 207 Pb/ 204 -Pb = 15.4891, and 206 Pb/ 204 -

Pb = 16.9356 after Todt (1996), using the method of White et al. (2000). For Pb, within-run (single day) precision is estimated from replicate measurements of SRM 981 (208 -Pb/ 204 Pb = 36.5840 \pm 7, 207 Pb/ 204 Pb = 15.4546 \pm 2, 206 -Pb/ 204 Pb = 16.9101 \pm 2, n = 21, 2SE). No blank corrections were applied as blank contributions were negligible (<0.1%): laboratory procedural blanks were <25 pg Hf, <90 pg Pb, <200 pg Nd and <250 pg Sr (see also Rooney et al., 2012).

2.3. Highly siderophile element abundances and Os isotopic analyses

Osmium isotope and highly siderophile element (HSE) abundance analyses were performed at the SIGL and at the University of Maryland, College Park (UMD). Samples were sealed in 20-cm long borosilicate Carius tubes, or in 50 mL Anton Paar high-pressure asher (HPA) quartz digestion vessels, with appropriate quantities of isotopically enriched multi-element spikes (⁹⁹Ru, ¹⁰⁶Pd, ¹⁸⁵Re, ¹⁹⁰Os, ¹⁹¹Ir, ¹⁹⁴Pt), and acid mixtures composed of 1 part 12 M HCl and 2 parts 16 M HNO₃. All reagents were quartz distilled and Teflon distilled, and HNO3 used for Os chemistry was multiply purged with H₂O₂ prior to distillation. Samples were digested in Carius tubes at a maximum temperature of 270 °C in an oven for >72 h, or in the Anton Paar HPA at 300 °C for >5 h. Osmium was triply extracted from the acid phase into CCl₄ (Cohen and Waters, 1996) and then back-extracted from the solvent into concentrated HBr, followed by purification using micro-distillation (Birck et al., 1997). The remaining HSE were recovered and purified from residual solutions using an anion exchange separation technique, prior to which desilicification was performed, in some instances (Day et al., 2016). Osmium isotopic compositions were measured as OsO₃ ions in negative ion mode using a *ThermoScientific* Triton thermal ionisation mass-spectrometer at the SIGL, or a ThermoFisher Triton thermal ionisation massspectrometer at UMD. All Os isotope masses were measured sequentially using an axial secondary electron multiplier. Possible Re contributions were monitored at masses 233 (185 ReO $_{3}^{-}$), 249 (185 ReO $_{4}^{-}$) and 251 (187 ReO $_{4}^{-}$). Signal at 233 was always found to be negligible (<5 cps), so Os ratios were not corrected for Re interference. Offline corrections of raw data for Os involved an oxide correction using ¹⁶O/¹⁸O and ¹⁷O/¹⁸O values from Nier (1950), an iterative fractionation correction (assuming the exponential law) using a ¹⁹²Os/¹⁸⁸Os ratio of 3.08271 (Shirey and Walker, 1998), a ¹⁹⁰Os spike subtraction, and blank contribution corrections. External precision of ¹⁸⁷Os/¹⁸⁸Os, determined by individual measurements of 3.5-35 pg Os standards (UMCP Johnson and Matthey) during the analytical campaign, was better than $\pm 2\%$ (187Os/188Os = 0.11371 ± 21 ; $n = 22; 2\sigma$).

Rhenium, Pd, Pt, Ru and Ir were measured using either: (1) a Cetac Aridus desolvating nebuliser coupled to a *ThermoFinnigan* Element 2 ICP-MS in low-resolution mode at UMD, or (2) using a *Thermo Scientific* iCAPQc ICP-MS at the *SIGL*. Isotopic ratios were corrected for mass fractionation using the deviation from the mean value of standards measured on the day of analysis, relative to the natural isotopic ratio for the element. Instrumental drift was negligible during analytical sessions. Solutions were monitored for possible oxide and elemental interferences

during analysis, but these were consistently found to be insignificant. External reproducibility (2σ) on more than 10 standard analyses for each analytical session was better than 0.2% for 0.01 to 1 ppb solutions of Re and Pt, 0.4% for Ir and better than 0.5% for Ru and Pd. Total procedural blanks (TPB) using both Carius tube and HPA digestion methods are broadly similar with an average \$^{187}Os/^{188}Os\$ of 0.17 ± 0.06 , and 0.22 ± 0.09 pg [Os], 2.2 ± 1.9 pg [Ir], $2.9 \pm 1.1 \text{ pg } [\text{Ru}], 15.4 \pm 18.3 \text{ pg } [\text{Pt}], 5.4 \pm 8.5 \text{ pg } [\text{Pd}],$ and 2.4 ± 3.8 pg [Re] (1 σ ; n = 4). All concentrations and isotopic compositions are corrected according to blank contributions measured for individually prepared experimental batches, resulting in a range of calculated uncertainties for samples. Accuracy and precision of standard data measured at the same time as samples are presented in Day et al. (2016).

3. RESULTS

We report sample descriptions and mineral modes in Table S1, and bulk-rock major- and trace-element compositions, ⁸⁷Sr/⁸⁶Sr, ¹⁴³Nd/¹⁴⁴Nd, ¹⁷⁶Hf/¹⁷⁷Hf, ²⁰⁸Pb/²⁰⁴Pb, ²⁰⁷Pb/²⁰⁴Pb, and ¹⁸⁷Os/¹⁸⁸Os ratios and HSE abundances on Azorean volcanic rocks and Mid-Atlantic Ridge samples in Tables 1–3.

3.1. Petrography and modal abundances

Volcanic samples from all the islands range from nearly aphanitic basalts to olivine-phyric basalts and ankaramites (clinopyroxene \geq olivine) (Fig. S1). We accurately determined mineral modes in the lavas, obtaining olivine/pyroxene ratios of \sim 0.3 to 0.6, with up to 6 modal % oxide and between 20 and 82 modal % matrix, or that can be highly vesicular (e.g., FA0802). Sulfide grains are rare to absent in some volcanic rocks. Where they do occur, the sulfide grains tend to be small (typically \leq 100 µm).

3.2. Major- and trace-element abundances

Sampled extrusive rocks are dominantly alkali basalts. olivine alkali basalts, or ankaramites, with minor trachybasalts and a single trachyandesite (Fig. S2). The sample suite that we examine displays major element differentiation trends characteristic of alkaline ocean island basalt suites and, of the Azores in particular (e.g., Flower et al., 1976; Self and Gunn, 1976; White et al., 1979; Widom and Shirey, 1996; Turner et al., 1997; Widom et al., 1997; França et al., 2006; Beier et al., 2006, 2007, 2008, 2010, 2012; Madureira et al., 2011; Zanon et al., 2013). For a given MgO content, São Miguel lavas typically have elevated TiO₂ and rare earth element (REE) abundances, lower Al₂O₃ contents, and higher Nb/Zr, Sm/Yb and Ce/ Pb than Pico or Faial lavas. Our data do not extend to the high Nb/Zr or low Ce/Pb reported for Santa Maria, Flores or Corvo (see Béguelin et al., 2017) (Fig. S3).

Primitive mantle-normalized incompatible trace element diagrams, grouped by island, are presented in Fig. 2. Volcanic rocks span a limited range of compositions, similar to previously published data for the islands (e.g., França et al., 2006; Beier et al., 2008). The patterns include relative depletions in Rb, K and Pb, with slight depletions in Th and U, relative to Nb. Overall, the lavas examined here have higher MgO, on average, than those previously stud-

Table 1 Major element and trace element abundances of lavas from São Miguel, Pico, Faial, and Terceira islands, Azores, measured by XRF and ICP-MS.

WAP9a , 28° 23.674		iel Pico			47.7	2.13	11.7		10.2	0.17	13.2	11.0	0.98	0.45		100.2	1.7/	5.20	32.8	161	1029	56	335	8. 28	12	9.61	422	20.7	28	0.22	292.0	23.0	6.20	25.3	5.77	1.76	0.77	4.28	0.82	2.02	0.29	0.24	4.07	1.99	0.21	0.67
SM0815 25°32.541	37°49.132′	el São Miguel	Agua de Pau		47.0	3.31	17.0	2.41 8.53	11.9	0.16	8.98	9.6	2.17	0.48	0.75	0.001	6.60	5.92	17.1	268	356	53	165	c 1	707	35.5	536	25.4	55	0.21	429.5	93.0	10.38	8.04	8.15	7.07	1.03	5.45	86.0	2.51	0.32	0.27	6.73	3.40	3.33	1.43
SM0814 25°30.950′	37°44.804′	São Miguel	e Agua de Pau		45.2	3.19	5.64	5.64 6.40	12.8	0.16	12.6	11.6	1.07	0.43	0.94	8.66	1.00	3.17	7.5	278	918	92	516	1/7	2 82	22.7	519	23.0	53	0.28	414.5	46.3 03.8	10.24	40.0	7.85	44.7	0.97	5.12	0.91	2.30	0.29	0.24	6.49	3.32	2.98	1.33
SM0813 25°40.576′	37°47.111′	São Miguel	Fissure Zone 2		45.0	3.01	12.0	5.33 6.14	12.2	0.17	11.7	11.2	1.15	0.48	1.15	9.66	0.50	4.38	26.8	288	927	57	255	93	61	27.0	578	23.0	49	0.24	431.6	32.7	8.58	34.8	7.28	2.36	7.02	4.87	0.88	2.25	0.28	0.24	4.90	3.04	3.44	0.94
SM0812 25°38.879′	37°47.994′	São Miguel	Fissure Zone 1	:	44.7	3.98	5.7	6.11 6.11	13.1	0.17	8.48	11.3	1.24	0.57	0.93	99.7	5.00	4.74	27.2	331	401	54	147	110	22	31.7	684	27.0	99	0.27	511.8	49.8 90.8	11.15	43.9	8.95	5.84 6.84	0.00	5.75	1.03	2.60	0.33	0.27	6.53	4.01	2.26	1.24
SM0811 25°33.871′	37°46.023′	São Miguel	Fissure Zone		45.0	4.08	12.1	3.39 8.80	13.4	0.17	16.6	11.5	1.43	0.46	0.78	100.0	C. CC	4.67	30.2	342	141	58	173	98	21	36.4	597	28.8	505	0.22	371.1	40.9	11.18	47.4	9.46	0.70	07.70	6.25	1.12	2.86	0.35	0.29	7.30	3.23	2.64	1.03
SM0810 25°29.779′	37°42.816′	São Miguel	ie Agua de Pau	4	48.0	3.44	2.35	3.25 7.22	11.3	0.16	7.00	8.88	2.87	0.65	0.64	100.0	7:00	6.21	20.9	311	234	43	135	107	24 /	59.2	789	29.7	99	0.54	875.3	56.9	13.99	55.3	10.16	5.63	1.19	6.25	1.10	2.81	0.35	0.30	7.96	3.95	4.00	1.55
SM0809 25°22.370′	37°45.510′		Fissure Zone 4	;	54.1	2.09	000	5.01	7.9	0.18	2.80	5.36	4.06	0.80	0.97	100.1	† †	12.68	7.9	147	2	6 .		4 1	29	105.6	365	48.4	148	0.46	1237.0	216.9	23.14	88.4	15.69	4.89	1.85	9.54	1.71	4.48	3.47	0.50	12.81	6.81	6.32	2.58
SM0808 25° 09.505′	37° 45.916′	São Miguel	Nordeste		46.8	3.6	2.67	3.9/ 7.89	12.7	0.17	6.65	8.59	1.95	0.53	2.43	8.66	97.0	11.33	23.8	381	279	47	122	12.	24 27	49.5	531	36.6	63	0.26	506.1	47.5	12.37	49.5	9.88	3.08	1.30	7.16	1.31	3.37	0.45	0.39	7.56	3.78	3.32	1.20
SM0807 25° 09.807'	37° 45.810′	São Miguel	Nordeste		1.8.1	3.71	10.0	4.8 <i>1</i> 6.69	12.2	0.16	4.52	7.90	2.24	0.64	1.87	8.66	7:7	12.26	21.7	376	9	38	20	67 7	27	58.3	919	38.9	77	0.20	668.2	137.0	14.51	56.9	11.15	3.44	1.10	7.77	1.40	3.72	0.47	0.41	8.48	4.54	3.56	1.42
SM0806 25°47.322'	37°48.331′	São Miguel	Sete de Cidades		46.1	3.14	2.01	3.01 7.84	11.7	0.17	10.9	11.5	1.22	0.50	0.70	99.8	Ć.	4.81	23.0	252	611	55	256	108	18	23.2	582	22.1 21.6	512	0.14	376.6	33.7	8.75	36.3	7.29	2.40	0.91	4.87	0.87	2.23	0.28	0.24	5.16	3.20	3.54	0.97
SM0805 25°47.427'	37°48.307′	São Miguel	Sete de Cidades		46.2	3.35	14:1	4.09 6.91	11.8	0.17	8.05	12.2	1.19	09.0	0.74	100.2	0.70	4.81	28.4	314	255	47	95	44	21	28.4	745	27.7	53	0.22	463.7	42.5 80.4	10.13	41.1	4.8	2.76	0.10	5.56	1.00	2.57	0.32	0.26	5.23	3.15	3.42	0.91
WASM33a SM0805 25°27.394′ 25°47.427	37°43.466′	São Miguel			45.6	3.34	0.11		12.6	0.17	12.0	10.1	1.38	0.87		100.2	5:50	5.30	22.7	246	1382	61	380	00	19	43.4	727	28.9	56	0.37	482.0	47.2	12.50	50.7	10.43	3.00	0.32	6.11	1.13	2.90	0.35	0.28	6.92	3.75	1.82	1.27
WASM32a 25°30.954′	37°45.664′	São Miguel			46.5	3.56	13.0		12.7	0.17	8.92	10.6 2 59	1.74	0.53		100.3	7.00	5.77	29.3	277	422	62	334	2/3	21	55.0	577	26.4	52	0.51	527.0	47.6 97.4	11.70	45.0	9.46	2.74	0.03	6.03	1.12	2.88	0.36	0.30	7.75	3.94	1.93	1.45
WASM1a WASM35a WASM24a 25°31.033′ 25°11.582′ 25°40.748′	37°47.356′	São Miguel			45.9	3.27	12.9		12.2	0.17	10.3	11.2	1.07	0.52		100.2	0.20	5.06	31.4	292	099	09	290	111	61	28.8	009	24.7	48	0.31	407.0	32.3	8.60	35.5	7.84	2.3/	0.95	5.08	96.0	2.50	0.31	0.25	5.12	3.24	3.60	1.02
WASMIa WASM35a 25°31.033′ 25°11.582′	37°43.860′ 37°50.982′	São Miguel			47.6	3.23	11		13.1	0.17	11.1	10.2 7.7.	1.39	0.46		100.5	0.5.7	6.82	26.4	566	488	89	321	100	16	34.1	456	29.9	44	0.16	342.0	36.7	9.60	41.1	9.12	75.7	1.15	6.12	1.18	3.05	0.38	0.33	6.63	3.03	1.39	1.15
WASM1a 25°31.033	37°43.860	São Miguel			45.8	3.34	0.71		13.0	0.18	11.2	10.8	1.53	4.0		100.5	1.50	5.39	29.8	274	743	67	367	001	61	36.4	297	27.2	52	0.36	404.0	40.4	10.80	43.7	9.28	2.69	1.11	5.79	1.09	2.78	20.34	0.28	66.9	3.56	0.95	1.27
SM0802B 25°49.336′	37°53.901′	São Miguel	Sete de Cidades		45.7	3.67	13.0	5.04	12.5	0.17	8.81	11.0	1.11	0.69	0.58	100.2	0.00	80.9	21.2	311	372	50	150	102	21	9.1	737	26.3	58	0.16	543.6	40.8	10.94	44.7	9.05	2.36 8.59	1.09	5.74	1.02	2.56	0.32	0.26	5.70	3.60	1.61	1.00
SM0802A 25°49.336′	37°53.901′	São Miguel	Sete de Cidades	(XRF)	45.4	3.75	0.51	4.54 7.11	12.4	0.17	8.54	11.1	1.31	69.0	0.61	7.66	5.VC	5.08	22.7	330	361	49	113	207	21	26.1	771	26.9 24.2	247	0.24	550.7	41.6 96.4	11.23	46.5	9.22	3.05 8.94	6.94 1.12	5.95	1.05	2.65	0.34	0.27	5.80	3.71	2.11	1.10
SM0801A 25°44.778′	37°49.160′	São Miguel	Fissure Zone Sete de 2 Cidades	Major Elements in weight % (XRF	46.0	2.87	2 67	5.8/ 6.96	11.6	0.16	12.2	12.0 7.27	0.99	0.45		0.001	J UCE	3.14	9.6	271	819	59	337	87 I	17	16.5	489	20.5	1 4	0.11	328.6	28.0	7.50	31.0	6.52	2.15	0.83	4.50	08.0	2.01	0.26	0.21	4.54	2.71	1.57	0.86
Sample ^a SM0801A Longitude (° 25°44.778' W)	Latitude (°N) 37°49.160'	Island	Locale	Major Element	SiO ₂	110 ₂	A1203	Fe_2O_3 FeO	Fe,O _{3T}	MnO	MgO	CaO	Na ₂ O K ₂ O	P_2O_5		Total	Trace elements	Li	Sc		C	ပိ ;	z d	Z. Z.	1 5	Rb	Sr	Y .	3 2	Cs	Ba	La Ce	P. P.	PN	Sm	na Eg	3 =	ζΩ	Ho	Er	E \$	Lu	Hſ	Ta Fi	윤부	n.

PX0805 PX	I	:			PX0810	PX0811	WAT3a	TR0801	TR0802	WAFlaa	FA0801	FA0802	FA0803	FA0805
5.411' 28°14.984' 28°13.315' 5.639' 38°23.435' 38°23.348'	28°14.984' 28°13.315' 38°23.435' 38°23.348'	28°13.315′ 38°23.348′		28°26.633′ 38°26.015′		28°32.449′ 38°30.383′		27°06.988′ 38°38.844′	6 6	.787	28°50.000′ 38°35.970′	28°44.486′ 38°44.486′	28°45.367′ 38°35.071′	28°49.299′ 38°35.185′
Pico Pico Pico S. Roque Topo Lajes	Pico Pico Topo Lajes Topo Lajes	Pico Topo Lajes		Pico Montanha	Pico Montanha		Terceira	Terceira	Terceira	Faial	Faial Capelinhos	Faial Cabeco Gorda	Faial da Cabeco Verde	
		0 1			,	,					t		ţ	
46.2 46.3 45.0 2.25 1.88 2.15		9.0		46.6	46.4	46.6	1 88		46.5	46.6	6.7	46.5	1./4	46.4
0.83		92.8		21.7	10.8	0.77			12.0	2.12 12.4	20.7	13.7	14.5	14.9
28.4		3.05		7 07	2 52	2.20			2.80	17:1	2.00	2.77	85 6	92.7
6.57		2.99		9.22	7.74	2.10			7.43		7.43	7.22	7.18	8.79
11.6		11.9		11.3	11.1	10.2			11.1	10.9	10.4	10.8	10.6	10.9
0.17		0.17		0.16	0.16	0.15	0.15		0.16	0.16	0.15	0.15	0.15	0.15
14.7		15.8		14.6	14.0	17.1			11.8	13.6	7.76	12.1	10.7	88.6
12.5		12.6		11.1	12.3	12.1			11.3	10.9	9.61	10.5	10.5	10.9
2.00		1.34		2.48	2.17	2.07			2.4	2.55	3.79	2.89	3.09	2.83
89.0		0.27		0.80	0.72	0.67			0.83	0.90	1.57	0.93	1.02	1.04
0.25		0.22		0.31	0.32	0.24			0.47	0.34	0.51	0.34	0.37	0.39
99.0		2.16		0.60	0.63	690			0.68	1001	0.65	0.74	49.0	6.75
71.5 72.4	72.4			71.9	71.3	0.001	70.6	56.5	67.9	71.1	59.8	2.00.7	66.8	89.1
4.23 4.43	4.43			4.87	4.63	4.52	4.35			4.83	5.31	4.98	5.16	4.56
16.3 25.5	25.5		. 64	10.1	29.7	14.9	30.9			33.3	21.6	18.0	18.3	21.1
267 249 267	267		4 ()	28	263	209	242	319	241	210	284	207	216	276
851 1033	1033		4.	999	929	1437	780			200	225	475	406	400
83	89			200	73	20	24			59	9	52	40	48
330 372	37.5			330	251	403	324			330	115	227	202	95
45		43		48	40	45				63	9	33	3.3	45
83		6		84	. 8	92	. 69			3 2	2 02		. 6	£ &
2		1 2		. 4	92	2 2	2 2			91	5 12	17	17	. <u>~</u>
0.6		1 0		152	17.5	11.7	23.0			17.9	30.8	11 6	13.6	13.0
318		365		3.62	275	324	381			410	5.07	453	452	490
16.4		20.7		19.1	23.6	16.8	20.0			20.5	25.4	21.0	22.1	22.4
133		147		139	169	120	127			143	. 171	169	178	182
24		27		27	30	21	26			26	46.	33	35	35
0.04		0.03		0.08	0.13	0.05	0.23			0.18	0.23	0.05	0.07	0.07
184.2		170.0		208.1	208.4	175.3				247.0	425.7	253.6	266.5	292.4
16.0		18.8		17.1	20.4	14.7				21.0	36.1	23.7	24.8	25.5
32.7		35.3		34.6	48.0	29.5				46.9	88.8	52.1	54.3	55.7
4.		5.29		4.78	5.89	4.15				5.70	9.11	6.44	6.74	7.06
18.8 22.2	22.7			20.0	25.2	17.4				23.9	36.0	27.2	27.9	29.0
7.69 4.23 5.05		5.05		04.40	2.67	10.4		7.42		5.59	.08	5.80	9.36	6.12
1.45		1.65		05.1	1.88	1.32				1.73	2.33	£ 5	0.7	2.11
6.35		5.19 6.79		4.55	2.77	80.4				/8.4	II./	5.90	20.0	6.24
0.01	0.72			t 9	0.81	0.39				77.0	56.0	0.81	0.83	0.84 6.84
3.45 4.03	4.03			3.69	4.56	3.32				4.29	2.05	4.47	4.56	4.69
0.64 0.76	0.76			89.0	0.84	0.62				0.84	0.94	0.82	0.85	0.87
1.66 1.95	1.95			1.83	2.21	1.60				2.06	2.46	2.11	2.20	2.25
0.21		0.25		0.24	0.28	0.21				0.28	0.32	0.28	0.29	0.29
1.29		1.50		1.45	1.74	1.30				1.71	1.95	1.65	1.72	1.78
0.18		0.20		0.21	0.24	0.18				0.24	28	0.24	0.25	0.25
3.74		3.51		3.25	4 02	2.78				3.84	5.45	4.07	4 33	444
1.47		19:01		1 66	181	1.76				182	07.0	2.05	2 13	100
7:1		1.00		1.00	1.01	1.20				70.1	2.70	1.03	2.12	17.7
1.10		CI:1		1 65	1.21	1.20				27.0	20.0	1.01	1.65	3.56
5.7		+								,				Z.:.70
		0.55		55.0	85.0	0.72				0.63	2.5	75.7	2.51	77.0

ied for Os isotopes by Schaefer et al. (2002) and Widom and Shirey (1996), with MgO ranging from 8.1 to 17.1 wt.% (average = 11.6 ± 4.8 wt.%, 2SD), but otherwise have major- and trace-element compositions similar to those previously reported for Azorean lavas (Flower et al., 1976; Self and Gunn, 1976; White et al., 1979; Widom and Shirey, 1996; Turner et al., 1997; Widom et al., 1997; Beier et al., 2006, 2007, 2008, 2010; França et al., 2006; Elliott et al., 2007; Madureira et al., 2011; Genske et al., 2016).

3.3. Strontium, Nd, Hf and Pb isotope compositions

Whole-rock Sr, Nd, Hf, and Pb isotopic compositions cover a similar range to those previously measured for Azores volcanic rocks (Hawkesworth et al., 1979; White et al., 1979; Turner et al., 1997; Widom et al., 1997; Beier et al., 2007, 2008, 2010, 2012; Elliott et al., 2007; Millet et al., 2009; Madureira et al., 2011; Genske et al., 2016; Béguelin et al., 2017) and thus, our sample set is representative of Azorean lava isotopic variability (Fig. 3). In particular, within our sample suite, ⁸⁷Sr/⁸⁶Sr and ¹⁴³Nd/¹⁴⁴Nd are negatively correlated among São Miguel, Faial, and Pico lavas, where São Miguel lavas trend to much higher ⁸⁷Sr/⁸⁶Sr (0.703341–0.70575) and lower ¹⁴³-Nd/¹⁴⁴Nd (0.51290–0.51268) and ¹⁷⁶Hf/¹⁷⁷Hf (0.283032– 0.282755) than lavas from either Pico (87 Sr/ 86 -Sr = 0.70354-0.70395, 143 Nd/ 144 Nd = 0.51292-0.51284, 176 Hf/ 177 Hf = 0.283052–0.283002) or Faial (87 Sr/ 86 -Sr = 0.70381–0.70403, 143 Nd/ 144 Nd = 0.51288–0.51284, 176 Hf/ 177 Hf = 0.282992–0.282937). The most enriched isotopic signatures are exclusively preserved in lavas from the easternmost sector of São Miguel Island, and these lavas have distinct ²⁰⁷Pb/²⁰⁴Pb and ²⁰⁸Pb/²⁰⁴Pb for a given ²⁰⁶Pb/²⁰⁴Pb ratio, compared to the rest of the Azores.

We measured only three samples from Terceira and they exhibit no clear correlation between ⁸⁷Sr/⁸⁶Sr and either ¹⁴³-Nd/144Nd or 176Hf/177Hf. Rather, Terceira lavas have 87- $Sr/^{86}Sr$ (0.70344–0.70353) similar to the most isotopically depleted Pico and São Miguel rocks and to literature data from Terceira (Turner et al., 1997; Beier et al., 2008; Madureira et al., 2011), but extend to more depleted ¹⁴³-Nd/¹⁴⁴Nd (0.51295–0.51291) and ¹⁷⁶Hf/¹⁷⁷Hf (0.283079– 0.283053) values. The most depleted samples from São Miguel have lower 176 Hf/ 177 Hf at the same 87 Sr/ 86 Sr as Pico, Faial, and Terceira lavas. The most enriched 176-Hf/¹⁷⁷Hf compositions, exhibited by São Miguel lavas, are akin to bulk silicate Earth (BSE) estimates but correspond to 143Nd/144Nd values (e.g., Beier et al., 2007; Elliott et al., 2007; Madureira et al., 2011) that are higher than the estimated BSE (e.g., Blichert-Toft and Albarède, 1997). This latter observation has previously been discussed by Elliott et al. (2007).

Lead isotopic compositions also cover a range in compositions akin to literature data from Azorean lavas (Turner et al., 1997; Beier et al., 2007, 2012; Elliott et al., 2007; Genske et al., 2016). São Miguel lavas have the largest range in Pb isotopic compositions, with ²⁰⁸Pb/²⁰⁴Pb = 39.24–40.39, ²⁰⁷Pb/²⁰⁴Pb = 15.59–15.80, and ²⁰⁶Pb/²⁰⁴Pb = 19.42–20.12 (Fig. 3d and e). As with previous data sets, Pb isotopic compositions in eastern and central São Miguel lavas extend above the northern hemisphere reference line (NHRL; Zindler and Hart, 1986). Pico lavas have a more limited range in ²⁰⁸Pb/²⁰⁴Pb (39.09–39.51) and ²⁰⁷Pb/²⁰⁴Pb (15.59–15.65) than São Miguel lavas, but have

variable ²⁰⁶Pb/²⁰⁴Pb (19.48–20.00), extending from values similar to the least radiogenic São Miguel lavas towards a traditional HIMU (high time-integrated ²³⁸U/²⁰⁴Pb) end member. In addition, despite their similar geographic and tectonic setting and similar Sr-Nd-Hf isotope compositions, Pico and Faial lavas exhibit different Pb isotopic characteristics, where Faial lavas have lower ²⁰⁶Pb/²⁰⁴Pb (19.27–19.64) and ²⁰⁸Pb/²⁰⁴Pb (39.11–39.27) compared with Pico lavas (²⁰⁶Pb/²⁰⁴Pb = 19.48–20.17, ²⁰⁸Pb/²⁰⁴Pb = 39.09–39.70), but similar, nearly constant ²⁰⁷Pb/²⁰⁴Pb. Relationships between Pb and Sr, Nd, and Hf isotopes reveal greater complexity than Sr, Nd, and Hf isotope systems alone. For example, Faial lavas show increasing ⁸⁷Sr/⁸⁶Sr and decreasing ¹⁴³Nd/¹⁴⁴Nd with increasing ²⁰⁶Pb/²⁰⁴Pb. The more limited samples analyzed from Terceira display Pb isotopic variability similar to Pico and Faial lavas, but at lower ²⁰⁸-Pb/²⁰⁴Pb and ²⁰⁷Pb/²⁰⁴Pb.

3.4. Highly Siderophile Element Abundances and ¹⁸⁷Os/¹⁸⁸Os

The most comprehensive database for ¹⁸⁷Os/¹⁸⁸Os and HSE abundances (Os, Ir, Ru, Pt, Pd, Re) for the Azores archipelago to date, spanning lavas from four islands, and using three different digestion methods, are reported in Table 3. Geographically related variations among HSE abundances are observed in the new data. Lavas from neighboring Pico and Faial have low, relatively homogeneous HSE abundances (total HSE abundances $\sim 0.001 \times \text{CI}$ chondrite; Ir = 0.014–0.133 ng g⁻¹). Lavas from Terceira and São Miguel, which are both situated along the Terceira Rift, have higher and more variable HSE abundances (total HSE = $\sim 0.003 \times CI$ chondrite; $Ir = 0.038-0.657 \text{ ng g}^{-1}$) (Fig. 4). The HSE have sloping patterns that are relatively depleted in Os, Ir, Ru and enriched in Pt, Pd, and Re, typical of mantle partial melts (Barnes et al., 1985; Rehkämper et al., 1999; Day, 2013). Pico and Faial lavas have lower and less variable chondrite-normalized $(Pd/Os)_N$ (average = 8.4 ± 10.5 [1SD]) than São Miguel and Terceira lavas (average (Pd/ $Os)_N = 26.5 \pm 13.8$ [1 σ]). Pico and Faial lavas also commonly lack the relative enrichment in Ir $(Ir/Ir_N^* = 1.1$ \pm 0.5 [1 σ], where Ir/Ir_N* = Ir_N/[$\sqrt{(Os_N \times Ru_N)}$]) observed in Terceira and São Miguel lavas (average Ir/Ir_N* = 2.5 \pm 1.2 [1 σ]). Notably, Ir enrichments in São Miguel and Terceira lavas are reminiscent of some OIB from the Canary Islands (Day et al., 2010), and contrast with Ir depletions present in Hawaiian picrites (Ireland et al., 2009), and some Juan Fernandez lavas (Paquet et al., 2019). Faial and Pico lavas have HSE patterns closer, but not identical in shape, to the Mid-Atlantic Ridge sample AII-0127-D44-1.

In general, Os, Ir, Ru, Pt, and Pd correlate with each other, but not with lithophile trace elements or Re. In detail, Ir shows strong to no correlation in the order of Pt $(R^2 = 0.9) > \text{Ru}$ $(R^2 = 0.64) > \text{Pd}$ $(R^2 = 0.58) > \text{Os}$ $(R^2 = 0.52) > \text{Re}$ $(R^2 = 0.1)$, that can be attributed to the individual Azorean islands having different Os, Ir and Ru inter-element relationships (e.g., Pico has lower Pd/Os than São Miguel). Although Re is lower in lavas with lower HSE abundances, Re poorly correlates with the HSE and covaries with lithophile incompatible elements (e.g., K₂O) (Fig. 5). In addition, São Miguel lavas have variable HSE abundances at similar MgO, resembling HSE systematics observed in western Canary Island lavas (Day et al.,

Table 2 Sr-Nd-Hf-Pb isotope data for Azores lavas.

1-111-0-1-10	o isotope data for Azotes lavas.	101 1200	os la vas.												Î
Sample	$^{87}\mathrm{Sr}/^{86}\mathrm{Sr}$	2σ	$^{143}{ m Nd}/^{144}{ m Nd}$	2σ	ϵNd	$^{176}{ m Hf/}^{177}{ m Hf}$	2σ	εHf	$^{208}\mathrm{Pb}/^{204}\mathrm{Pb}$	2σ	$^{207}\mathrm{Pb/^{204}Pb}$	2σ	$^{206}{ m Pb}/^{204}{ m Pb}$	2σ	Measurement
SM0804X	0.703341	0.000003	0.512897	0.000003	5.0	0.283032	0.000004	9.2	39.147	0.0012	15.587	0.0004	19.395	0.0004	SIGT/SDSU
WASM1a ^a	0.70448		0.51274		2.0				40.106		15.730		19.892		MUO
WASM35 ^a	0.70575		0.51268		0.8				40.345		15.785		20.094		MUO
WASM24 ^a	0.70352		0.51289		6.4				39.353		15.604		19.533		MUO
$WASM32^{a}$	0.70491		0.51273		1.8				40.045		15.729		19.828		MUO
WASM33 ^a	0.70478		0.51273		1.8				40.128		15.738		19.908		MUO
SM0803	0.703516	0.000005	0.512887	0.000002	4.9	0.282994	0.000002	7.9	39.312	0.0007	15.600	0.0002	19.427	0.0002	SIGT/SDSU
SM0805	0.703510	0.000004	0.512898	0.000003	5.1	0.283008	0.000002	8.3	39.307	0.0000	15.599	0.0003	19.500	0.0003	SIGE/SDSU
8M0806	0.703434	0.000003	0.512893	0.000005	5.0	0.282999	0.000003	8.0	39.237	9000.0	15.592	0.0002	19.420	0.0002	SIGE/SDSU
SM0807	0.705651	0.000003				0.282782	0.000002	0.3	40.326	0.0010	15.768	0.0003	20.023	0.0003	SIGT/SDSU
SM0808	0.705345	0.000004	0.512678	0.000005	8.0	0.282755	0.000002	-0.6	40.352	0.0007	15.769	0.0002	20.099	0.0002	SIGT/SDSU
SM0809	0.704856	0.000007	0.512735	0.000003	1.9	0.282821	0.000002	1.7	40.149	0.0004	15.736	0.0002	19.951	0.0002	SIGT/SDSU
SM0810	0.705206	0.000005	0.512705	0.000002	1.3	0.282770	0.000002	-0.1	40.274	0.0008	15.755	0.0003	19.965	0.0003	SIGT/SDSU
SM0811	0.705158	0.000003	0.512711	0.000003	1.4	0.282792	0.000002	0.7	40.392	0.0008	15.803	0.0002	20.123	0.0002	SIGT/SDSU
SM0812	0.703869	0.000005	0.512842	0.000002	4.0	0.282938	0.000001	5.9	39.655	9000.0	15.651	0.0002	19.664	0.0002	SIGT/SDSU
SM0813	0.703524	0.000004	0.512890	0.000005	4.9	0.282983	0.000002	7.5	39.341	0.0006	15.601	0.0002	19.501	0.0002	SIGT/SDSU
SM0814	0.705210	0.000003				0.282763	0.000002	-0.3	40.366	0.0005	15.768	0.0002	19.980	0.0002	SIGT/SDSU
SM0815	0.704641	0.000005	0.512736	0.000003	1.9	0.282828	0.000002	2.0	40.137	0.0005	15.729	0.0002	19.889	0.0002	SIGT/SDSU
$WAP9^a$	0.70393		0.51284		3.9				39.093		15.588		19.476		MUO
$WAP25^{a}$	0.70382		0.51287		4.5				39.366		15.604		19.899		MUO
PX0801	0.703753	0.000003	0.512860	0.000003					39.388	0.0005	15.637	0.0002	19.969	0.0002	SIGT/SDSU
PX0802	0.703801	0.000003	0.512884	0.000003	8.8	0.283004	0.000002	8.2	39.389	9000.0	15.639	0.0003	19.804	0.0003	SIGT/SDSU
PX0803	0.703775	0.000003				0.283009	0.000002	8.4	39.442	0.0006	15.646	0.0005	19.909	0.0007	SIGT/SDSU
PX0804	0.703773	0.000003							39.469	0.0004	15.649	0.0002	19.918	0.0002	SIGT/SDSU
PX0805	0.703789	0.000003	0.512879	0.000002	4.7	0.283002	0.000002	8.1	39.443	0.0004	15.641	0.0001	19.804	0.0002	SIGT/SDSU
PX0806	0.703537	0.000002	0.512918	0.000002	5.5	0.283013	0.000002	8.5	39.366	0.0005	15.627	0.0002	19.963	0.0002	SIGT/SDSU
PX0807	0.703820	0.000002				0.283008	0.000003	8.4	39.533	0.0008	15.654	0.0002	19.929	0.0003	SIGT/SDSU
PX0808	0.703947	0.000003							39.502	0.0005	15.645	0.0002	19.873	0.0002	SIGT/SDSU
PX0809	0.703743	0.000003				0.283028	0.000003	0.6	39.379	0.0004	15.635	0.0001	19.955	0.0002	SIGT/SDSU
PX0810	0.703626	0.000004				0.283032	0.000002	9.2	39.509	0.0005	15.643	0.0002	20.003	0.0002	SIGT/SDSU
PX0811	0.703672	0.000003				0.283052	0.000002	6.6	39.702	0.0004	15.669	0.0002	20.175	0.0002	SIGT/SDSU
$WAT3^a$	0.70344		0.51291		5.3				39.272		15.605		19.768		MUO
TR0801	0.703531	0.000012	0.512953	0.000003	6.1	0.283079	0.000002	10.9	39.121	0.0011	15.589	0.0004	19.754	0.0004	SIGT/SDSU
TR0802	0.703478	0.000006	0.512938	0.000003	5.8	0.283053	0.000002	6.6	38.892	0.0009	15.545	0.0003	19.311	0.0003	SIGT/SDSU
$WAF1a^a$	0.70388		0.51286		4.3				39.262		15.628		19.579		MUO
FA0801	0.704028	0.000006	0.512835	0.000002	3.8	0.282937	0.000002	5.8	39.107	0.0006	15.631	0.0002	19.273	0.0002	SIGT/SDSU
FA0802	0.703830	0.000004	0.512875	0.000003	4.6	0.282986	0.000002	9.7	39.265	0.0005	15.637	0.0002	19.643	0.0002	SIGT/SDSU
FA0803	0.703814	0.000005	0.512881	0.000003	4.7	0.282992	0.000002	7.8	39.253	0.0005	15.635	0.0002	19.621	0.0002	SIGT/SDSU
FA0805	0.703935	0.000004	0.512877	0.000002	4.7	0.282983	0.000002	7.5	39.192	0.0005	15.627	0.0002	19.447	0.0002	SIGL/SDSU

^a Data from Miami University (Ohio) reported in Yu (2011).

Table 3 Highly siderophile element (ng $\rm g^{-1}$) and $\rm ^{187}Os/^{188}Os$ isotope compositions of Azores lavas.

Location	Sample	MgO (wt.%)	Fo	$\pm 2\sigma$	Os	Ir	Ru	Pt	Pd	Re	¹⁸⁷ Os/ ¹⁸⁸ Os	$\pm 2\sigma$	Method
São Miguel	WASM1a	11.2			0.152	0.371	0.286	2.689	6.585	0.353	0.13139	0.00007	CT
	WASM5	11.1			0.046	0.168	0.120	1.097	1.852	0.279	0.16025	0.00017	CT
	WASM24	10.3			0.149	0.410	0.204	3.007	2.679	0.226	0.12568	0.00007	CT
	WASM32	8.9			0.283	0.652	0.438	5.109	6.538	0.432	0.12931	0.00007	CT
	WASM33	12.0			0.111	0.190	0.223	1.232	1.626	0.341	0.12879	0.00009	CT
	SM0805	8.1			0.014	0.067	0.020	0.566	0.541	0.315	0.1317	0.0020	CT
	SM0806	10.9	87.4	0.6	0.048	0.657		4.185	2.783	0.196	0.12668	0.00009	HPA ^b
					0.044	0.314		3.398	2.973	0.232	0.12668	0.00007	HPA ^b
					0.068	0.448	0.277	3.438	4.327	0.209	0.12689	0.00031	CT ^b
	~~ ~~ ~~ ~~ ~~ ~~ ~~ ~~					0.490	0.234	3.943	3.311	0.260			CT-HF ^b
	SM0811	9.9	83.1	3.2	0.069	0.133	0.137	1.167	1.150	0.360	0.12789	0.00016	CT ^b
					0.069	0.100	0.040	1 000	1 2 4 5	0.240	0.12936	0.00018	HPA ^b
					0.069	0.128	0.243	1.099	1.247	0.249	0.13021	0.00116	CT ^b
	G3 40012	0.5	01.1		0.026	0.163	0.101	1.161	3.444	0.431	0.12001	0.00004	CT-HF ^b
	SM0812	8.5	81.1	6.5	0.036	0.118	0.199	1.090	1.170	0.311	0.12901	0.00084	CT^b
					0.067	0.110	0.212	1 000	1 442	0.210	0.12860	0.00057	HPA ^b CT ^b
					0.040	0.119	0.213	1.808	1.442	0.210	0.13020	0.00052	CT-HF ^b
	CM0012	11.7	86.4	1.2	0.033	0.159	0.172 0.118	1.148	3.903 2.046	0.318 0.214	0.13262	0.00029	CT-HF CT
	SM0813 SM0814	11.7 12.6	80.4	1.2	0.033	0.227 0.526	0.118	2.090 4.683	3.385	0.214	0.13262	0.00029	CT
	SM0814 SM0815	9.0			0.243	0.326	0.466	0.739	0.709	0.313	0.13130	0.00003	CT
		9.0				0.071		0.739	0.709	0.240			
Pico	WAP9	13.2			0.050	0.078	0.105	0.315	0.685	0.163	0.12369	0.00009	CT
	WAP25	14.4			0.038	0.082	0.110	0.354	1.509	0.120	0.12454	0.00007	CT
	PX0801	16.5	87.0	2.2	0.016	0.024	0.035	0.296	0.241	0.066	0.12427	0.00022	CT^b
					0.029	0.016	0.122	0.692	0.698	0.226	0.12466	0.00091	CT ^b
						0.015	0.173	0.227	1.185	0.092			CT-HF ^b
	PX0802	9.6	82.5	2.8	0.055	0.047	0.070	0.260	0.190	0.156	0.1246	0.0013	CT
	PX0804	17.1	86.7	1.0	0.078	0.029	0.058	0.184	0.133	0.064	0.1261	0.0011	CT ^b
					0.026	0.024		0.171	0.125	0.053	0.12588	0.00010	HPA ^b
					0.037	0.044	0.193	1.123	1.775	0.306	0.12635	0.00027	CT ^b
	D110005	11.5			0.005	0.039	0.169	0.661	1.424	0.109	0.10.100	0.00014	CT-HF ^b
	PX0805	11.7			0.085	0.037	0.074	0.239	0.175	0.108	0.12408	0.00014	CT
	PX0808	15.8			0.057	0.057	0.174	0.376	0.161	0.041	0.12816	0.00009	CT
	PX0810	14.0			0.039	0.073	0.041	0.354	0.190	0.099	0.1337	0.0011	CT CT ^b
	P5	9.6			0.015	0.029	0.193	1.184	2.944	0.267	0.12611	0.00020	
					0.037	0.007	0.032	0.182	1.213	0.155 0.043	0.12012	0.00017	CT-HF ^b CT ^c
					0.037					0.043	0.12012	0.00017	
Terceira	WAT3	11.7			0.107	0.248	0.187	2.238	2.881	0.148	0.12297	0.00006	CT
	TR0801	8.1			0.012	0.038		0.479	0.317	0.247	0.12786	0.00022	CT^{b}
					0.042	0.064	0.055	0.497	0.491	0.275	0.1264	0.00188	HPA^b
					0.015	0.045	0.048	0.570	1.173	0.279	0.13097	0.00091	CT^b
						0.041	0.049	0.874	1.852	0.265			CT-HF ^b
	TR0802	11.8	83.0	5.1	0.032	0.041	0.076	0.457	0.607	0.189	0.13840	0.00272	CT
Faial	WAF1a	13.6			0.116	0.133	0.248	1.190	1.800	0.157	0.12626	0.00008	CT
	FA0802	12.1				0.018	0.031	0.169	0.108	0.106			CT
	FA0803	10.7	80.9	6.1	0.016	0.014	0.011	0.130	0.092	0.106	0.1350	0.0017	CT
	FA0805	9.9	81.8	2.2	0.035	0.031	0.039	0.209	0.180	0.181	0.12530	0.00019	CT
	F/CA 6	9.7			0.028	0.027	0.176	0.545	1.016	0.329	0.13086	0.00072	CT^b
						0.036	0.068	0.205	1.005	0.204			CT-HF ^b
					0.016					0.150	0.11019	0.00039	CT^c
MAR	AII-0127-Ε	044-1			0.025	0.022	0.044	0.360	1.648	0.624	0.2842	0.0013	CT
171/111	AII-0127-E				0.023	0.022	0.020	1.841	2.127	0.624	0.2642	0.0013	CT
	AH-012/-L	CT ^b Carina 4			0.019	0.000	0.020	T 4:1:			U.1343	0.0021	<u> </u>

CT = Carius tube UMD; CT^b = Carius tube SIGL; CT-HF b = Carius tube & HF desilicification SIGL; HPA^b = high-pressure asher SIGL; CT^c = Carius tube, Schaefer et al. (2002). External precision on HSE abundances from solutions is better than 0.5%.

2010). By contrast, Pico lavas have lower HSE abundances (most clearly Pt and Ir) that increase with decreasing MgO from \sim 17 wt.%, reach a maximum at \sim 14 wt.% MgO, and

then decrease at lower MgO contents (Fig. 6). These relationships result in lower Pd/Os and Ir/Ir* in Pico and Faial lavas relative to São Miguel and Terceira lavas.

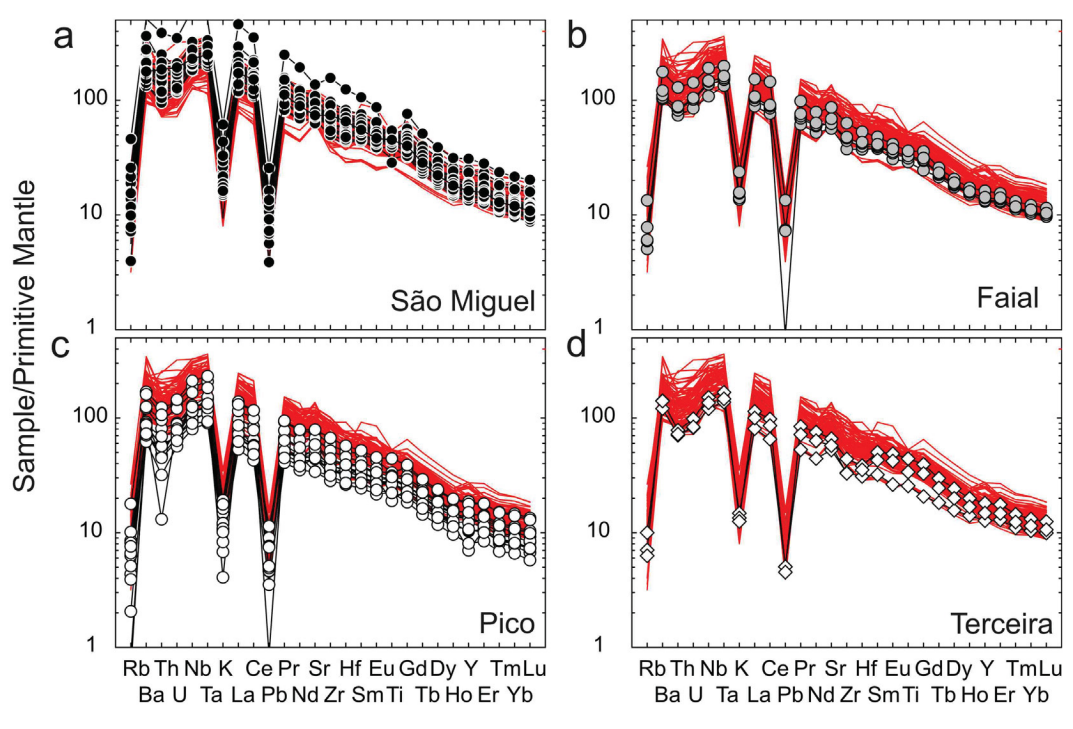


Fig. 2. Primitive mantle-normalized incompatible trace element (ITE) patterns for (a) São Miguel lavas; (b) Faial lavas; (c) Pico lavas and (d) Terceira lavas. Solid lines without symbols denote published Azores lava data from the GEOROC database. Primitive mantle normalization from McDonough and Sun (1995). (For interpretation of the references to color in this figure legend, the reader is referred to the web version of this article.)

Osmium isotope compositions for São Miguel (range = 0.1257–0.1603, average = 0.132 ± 0.010 [1 σ], n = 12) and Terceira lavas (range = 0.1230–0.1384, average = 0.130 ± 0.08 [1 σ], n = 3) are, on average, more radiogenic and exhibit greater dispersion than Pico $(range = 0.1237 - 0.1337, average = 0.126 \pm 0.004 [1 \sigma],$ n = 9) or Faial lavas (range = 0.1253–0.1350, average = 0.129 ± 0.06 [1 σ], n = 5) (Fig. 7). The range in Os isotopic compositions that we report is broadly similar to published analyses for Faial, Pico, São Miguel and Terceira by Widom and Shirey (1996), but does not extend to the unradiogenic ¹⁸⁷Os/¹⁸⁸Os ratios for Pico and Faial reported by Schaefer et al. (2002). Our re-analysis of the most unradiogenic samples from Schaefer et al. (2002) did not reproduce the original values (Pico P5 187 Os/ 188 Os = 0.1261; Faial F/CA6 = 0.1309; Table 1), which likely reflects analytical artefacts with the originally reported data (Day et al., 2016). Osmium isotope compositions, HSE abundances, and HSE ratios do not correlate well with Sr, Nd, Hf, or Pb isotope compositions, nor does ¹⁸⁷Os/¹⁸⁸Os correlate well with HSE abundances or HSE inter-element ratios (Fig. 8). Moreover, though not correlated, lavas with higher ¹⁸⁷Os/¹⁸⁸Os tend towards more radiogenic lithophile isotopic compositions and greater Ir/Ir_N* in the sample suite. Because of their geochemical and geographical/tectonic similarities, we group Pico and Faial lavas, and São Miguel and Terceira lavas together in the discussion.

4. DISCUSSION

Elemental abundances and Sr-Nd-Hf-Pb isotope data for the studied Azorean samples span a similar range to previously published data for the same islands. The samples analyzed for HSE abundances and Os isotope compositions can, therefore, be considered as representative of the geochemical variability of lavas from São Miguel, Terceira, Faial, and Pico. São Miguel lithophile elemental compositions are consistent with contributions from a long-term enriched mantle source component of either metasomatic or recycled crustal origins, as discussed previously (cf., Beier et al., 2007; Elliott et al., 2007), whereas Pico and Faial lavas indicate a relatively more depleted source, trending between a more MORB-like composition and a HIMU-like end member. We focus our discussion on processes leading to HSE abundance and Os isotope compositional variations in Azorean lavas, and how these data relate to existing and extensive interpretations of lithophile element and isotopic data. Ultimately, we examine how the lack of relationship among lithophile and siderophile systems can occur, due to the different mineral phases that they are hosted within and the important role of silicate versus sulfide melting in basalt genesis.

4.1. No role for assimilation processes

The Azores volcanic rocks in this study are more primitive or accumulative, on average, than those previously studied for Os isotopes by Schaefer et al. (2002) and Widom and Shirey (1996). Their HSE compositions provide a more robust record of mantle source characteristics, if crystallization and assimilation effects can be isolated from those of partial melting and mantle source heterogeneity. Evidence for assimilation of syenite in some São Miguel lavas has been previously documented (e.g., Widom and Shirey, 1996; Widom et al., 1997; Elliott et al., 2007;

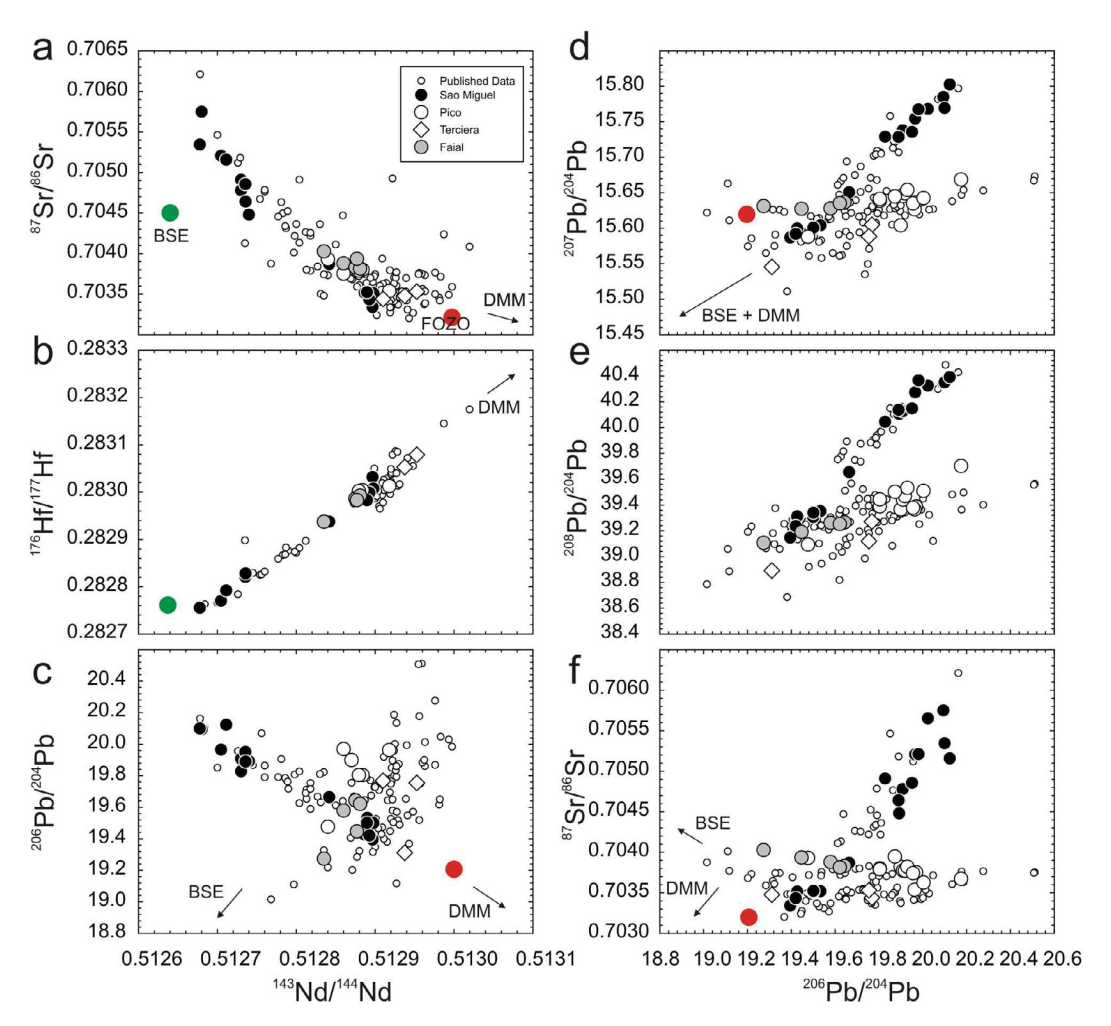


Fig. 3. Plots of 143 Nd/ 144 Nd versus (a) 87 Sr/ 86 Sr, (b) 176 Hf/ 177 Hf, (c) 206 Pb/ 204 Pb and 206 Pb/ 204 Pb versus (d) 207 Pb/ 204 Pb, (e) 208 Pb/ 204 Pb and 87 Sr/ 86 Sr for Azores lavas compared with published data from Widom et al. (1997), Beier et al. (2007, 2008), Elliott et al. (2007) and Millet et al. (2009). Estimates of FOZO, bulk silicate Earth (BSE) and depleted MORB mantle (DMM) taken from Day et al. (2010). Uncertainties are generally smaller than symbols.

Prytulak et al., 2014), and contamination by mantle lithosphere has also been demonstrated for some OIB lavas (e.g., Widom et al., 1999). Crustal contamination played a sub-ordinate role over melting processes and source heterogeneity in controlling ¹⁸⁷Os/¹⁸⁸Os and HSE abundance variations in the presented dataset based on two observations. First, there is a lack of correlation between Os isotopes and Os abundances in the sample suite, particularly in samples with <50 pg g⁻¹ Os, which would be more susceptible to contaminants with comparatively high HSE abundances (cf. Widom and Shirey, 1996) (Fig. 7). This conclusion is supported by the observation that assimilation of crustal material with distinct HSE abundances and more radiogenic ¹⁸⁷Os/¹⁸⁸Os generally has a dilutional effect on HSE abundances (Ireland et al., 2009). Second, mantle and cumulate xenoliths typically have characteristic traceelement compositions, highly distinct from the volcanic rocks and have high Cr and Ni contents, making contamination by these materials unlikely (e.g., Widom et al., 1999; Day, 2013). Mantle lithosphere generally has unradiogenic

¹⁸⁷Os/¹⁸⁸Os and high Os contents, also ruling this reservoir out as a potential contaminant to Azorean lavas (Fig. S4). Assimilation of crustal or lithospheric mantle materials is not responsible for differences in relative HSE abundances between São Miguel and Pico lava compositions since São Miguel has more radiogenic ¹⁸⁷Os/¹⁸⁸Os yet higher HSE abundances.

4.2. Crystallization modeling of Azorean parental melts

Sulfide crystallization or accumulation has a first order control on HSE compositions of even primitive OIB lavas (Day, 2013; Gannoun et al., 2016). We observe correlations of HSE consistent with such processes within individual Azorean islands. The Pico (and Faial) and São Miguel (and Terceira) lava suites define distinct liquid lines of descent in plots of MgO versus HSE abundances, with São Miguel lavas having roughly two to five times higher abundances than Pico lavas at the same MgO. This indicates that each suite requires different HSE concentrations in their

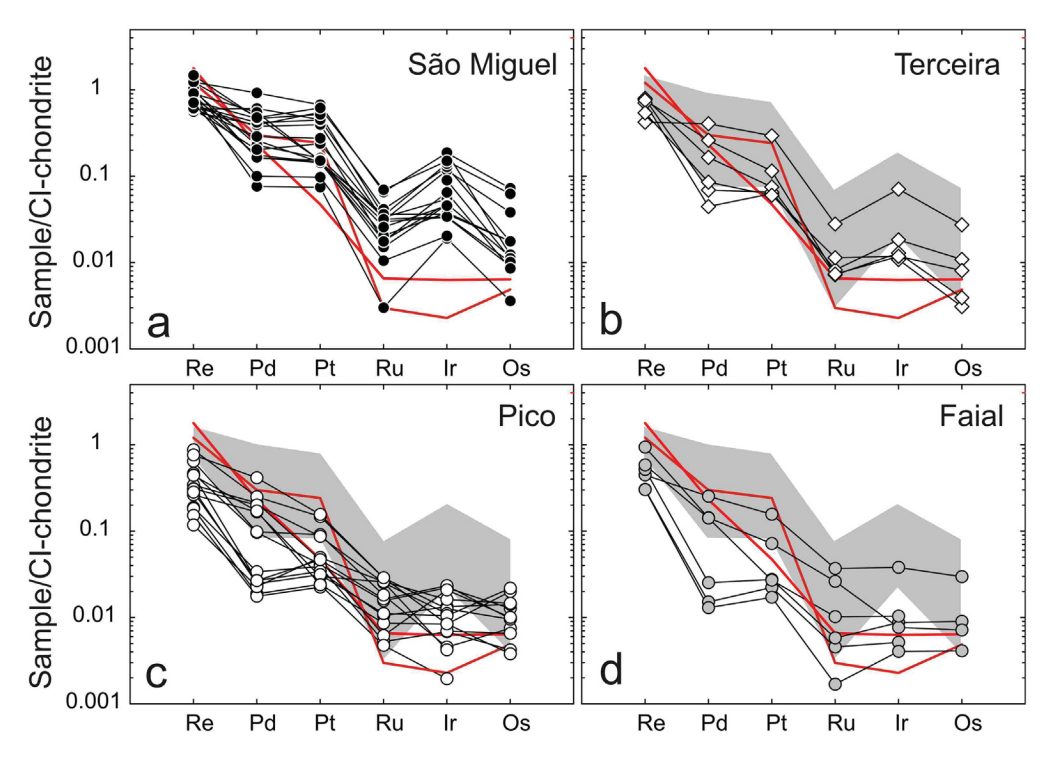


Fig. 4. Chondrite-normalized highly siderophile element abundance patterns of lavas from (a) São Miguel and (b) Terceira islands and (c) Pico and (d) Faial islands. There is no recognizable difference in HSE pattern with longitude in São Miguel. Normalization values from Day et al. (2016). The grey field shows the range of abundances for São Miguel lavas. Solid lines without symbols denote the Mid-Atlantic Ridge sample AII-0127-D44-1. (For interpretation of the references to color in this figure legend, the reader is referred to the web version of this article.)

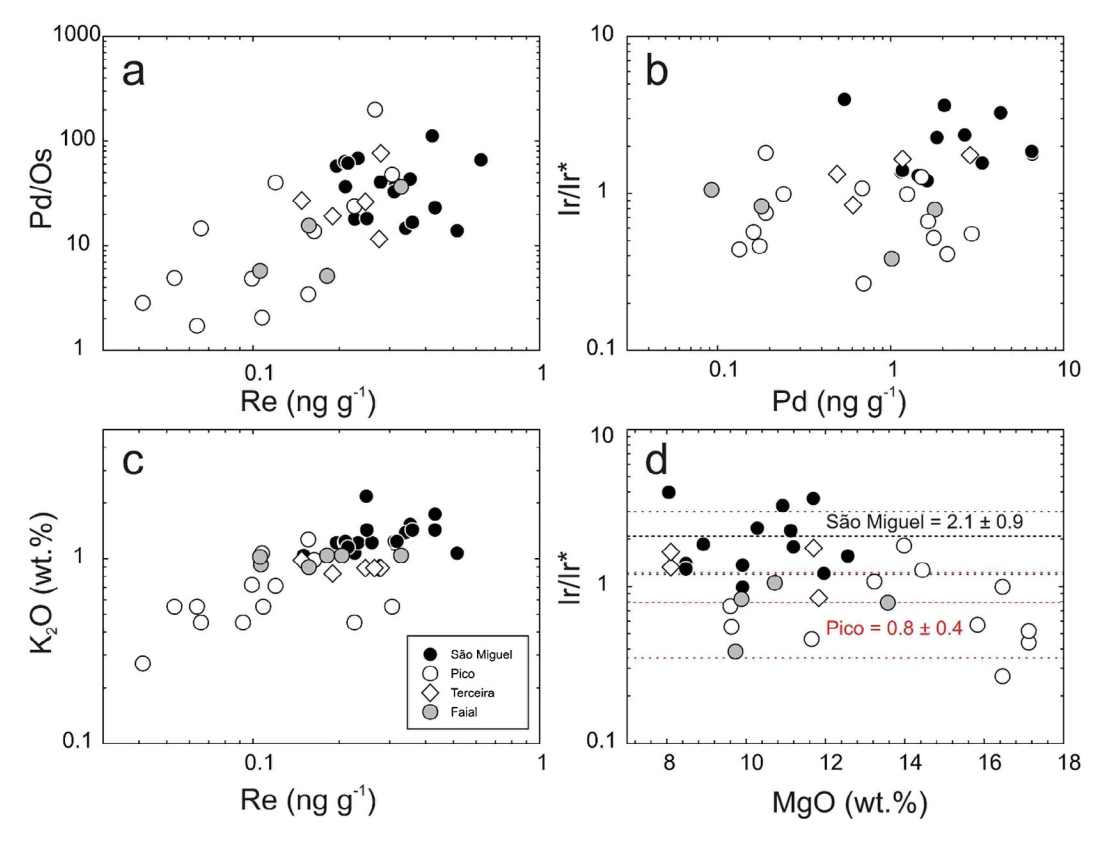


Fig. 5. Variations of (a) Re versus Pd/Os; (b) Ir/Ir^* versus Pd; (c) Re versus K_2O and (d) MgO versus Ir/Ir^* . Closely spaced stippled lines and stippled lines in (d) denote average and standard deviations of Ir/Ir^* measured in São Miguel and Pico.

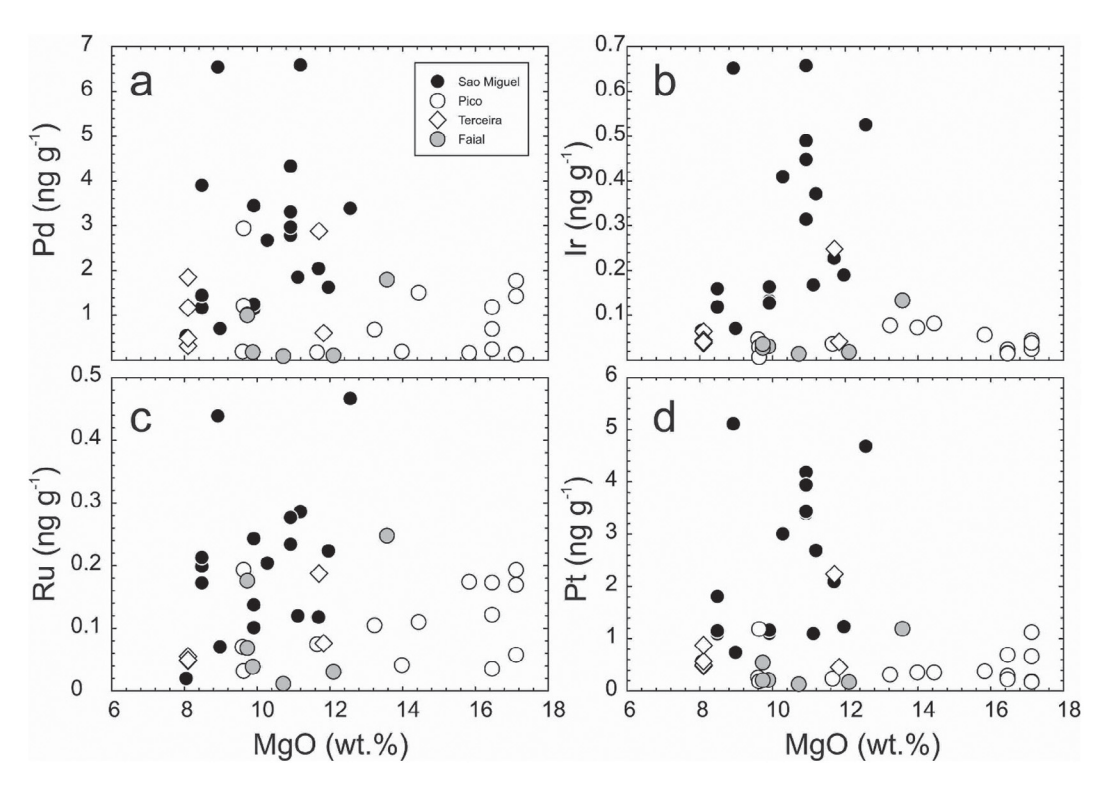


Fig. 6. Variations of MgO versus (a) Pd, (b) Ir, (c) Ru and (d) Pt in Azorean volcanic rocks.

parental melt (Figs. 4 and 6). To estimate the effects of fractional crystallization on MgO contents, the thermodynamically constrained software MELTS (Ghiorso and Sack, 1995), was used to reproduce the liquid line of descent (LLD) for Pico lavas. Using the results from MELTS, we determined equations that described MgO as a function of F (Fig. S5). Crystallization of different phases was approximated (e.g., olivine, then clinopyroxene + olivine, then olivine + clinopyroxene + plagioclase) by MELTS over discrete intervals of MgO using different linear and polynomial equations, and so can be used for fractional crystallization calculations to determine HSE abundances.

To simulate effects of crystallization processes on HSE abundances, a model of fractional crystallization of 50% olivine, 49.9% clinopyroxene, and 0.1% sulfide was assumed. Olivine, clinopyroxene, and sulfide are all minerals that are expected to crystallize at MgO >8 wt.%, and for which there are available experimental partitioning data (Puchtel and Humayun, 2001; Chazey and Neal, 2005; Brenan et al., 2012; Day, 2013). The low sulfide content is generally consistent with typical sulfide abundances observed in polished thin sections. The relative proportions of olivine and clinopyroxene have limited effect on the HSE liquid line of descent, compared to sulfide. Mineral/melt partition coefficients and other modeling parameters are summarized in Tables S2 and S3.

A parental melt composition equivalent to the WAP9 composition was used. This is a Pico lava with 13.2 wt.% MgO, similar to estimates of parental melt MgO (Beier et al., 2008). Successful PRIMELT3 (Herzberg and Asimow, 2015) calculations of sample compositions that have lost or gained olivine support these estimates, with predicted parental melt compositions of between 14 and

16 wt.% MgO, in equilibrium with Fo_{90.6-91} olivine and mantle potential temperatures of 1415-1470 °C under anhydrous conditions. Previously, Beier et al. (2012) constrained a low solidus temperature in the Azores, requiring at least 200 ppm H₂O in the mantle, and excess mantle temperatures <100 °C, consistent with our calculations and those of Métrich et al. (2014). Observed major element trends for Pico lavas are reproduced by MELTS modeling for crystallization of WAP9 at 3 kb, and HSE abundance variations in Pico lavas are reproduced by Rayleigh crystallization modelling of sulfide with olivine and then with olivine + clinopyroxene (Fig. 9). Decrease in HSE abundances for most lavas above 14 wt.% MgO likely results from a dilution effect by olivine and clinopyroxene crystal accumulation, where the relative proportions of these two phases have no effect on HSE liquid lines of descent (LLD). If primitive São Miguel lava, SM0814, is used for a parental melt composition, fractional crystallization (at 5 kb) can reproduce the broad variations observed in São Miguel lavas (through ~30% crystallization), although the absolute percent crystallization needed to explain the data is subject to variations in the proportion of sulfide crystallizing. For example, an increase to 0.3% sulfide decreases F to just \sim 15%, although there is a predicted decrease in Pd, relative to Pt and Re, which does not occur in the measured

The HSE abundance variations within each suite are reproduced by modeling crystallization of sulfide from compositionally distinct parental melts for Pico/Faial lavas and São Miguel/Terceira lavas (Fig. 9). It is, however, impossible to generate Pico and Faial lava HSE compositions by crystallization of a parental melt composition like that required for São Miguel, or vice versa. Although

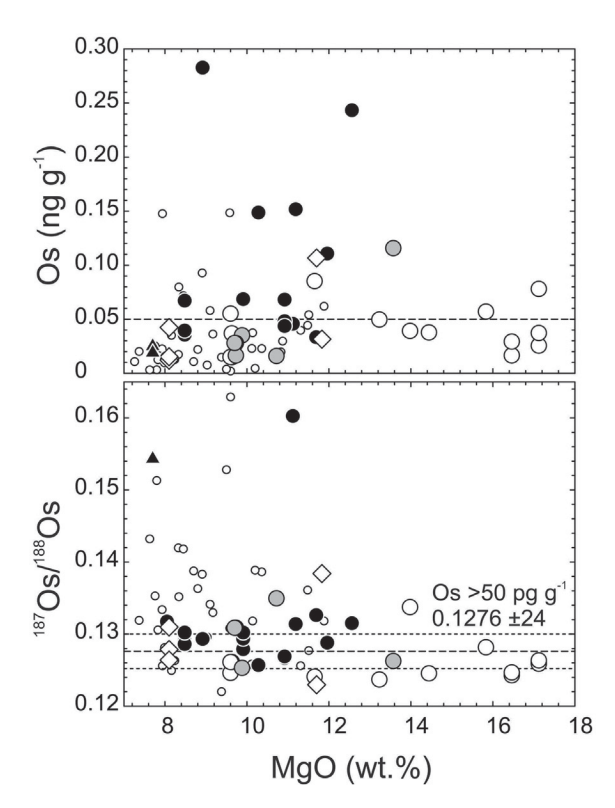


Fig. 7. MgO versus Os concentration and $^{187}\text{Os}/^{188}\text{Os}$ in Azores lavas from this study and the literature (small unfilled circles; Widom and Shirey, 1996; Schaefer et al., 2002). Using only lavas with >50 pg g $^{-1}$ Os (stippled line in upper panel) from this study gives an average $^{187}\text{Os}/^{188}\text{Os}$ of 0.1276 ± 0.0024 (solid line, with standard deviations shown as stippled lines in lower panel). Symbols same as for Fig. 3.

crystallization of different base-metal sulfides or HSE-bearing sulfides or alloys can change the trajectory of the LLD within a suite, sulfide and/or alloy crystallization cannot account for the two to five times higher HSE abundances for São Miguel versus Pico lavas at a given MgO content. Similarly, crystallization of a parental melt of São Miguel or Terceira composition cannot reproduce HSE inter-element fractionations between the island groups.

4.3. Melting of a homogeneous mantle source of primitive mantle sulfide composition

To model the range of possible effects of partial melting of a homogeneous source in the convecting mantle, we use both the melt entrainment model (e.g., Bockrath et al., 2004; Ballhaus et al., 2006), where sulfide-sulfide melt partitioning governs HSE abundances, and a fractional melting model where silicate melt-sulfide melt partitioning controls HSE abundances (e.g., Mungall and Brenan, 2014). When modeling silicate melting systems, HSE partitioning between silicate and sulfide melts, and between monosulfide and sulfide melts, is not as well understood as for lithophile element systems (Brenan et al., 2016). Nonetheless, partition coefficients for the HSE between monosulfide and sulfide melts (Ballhaus et al., 2006) and

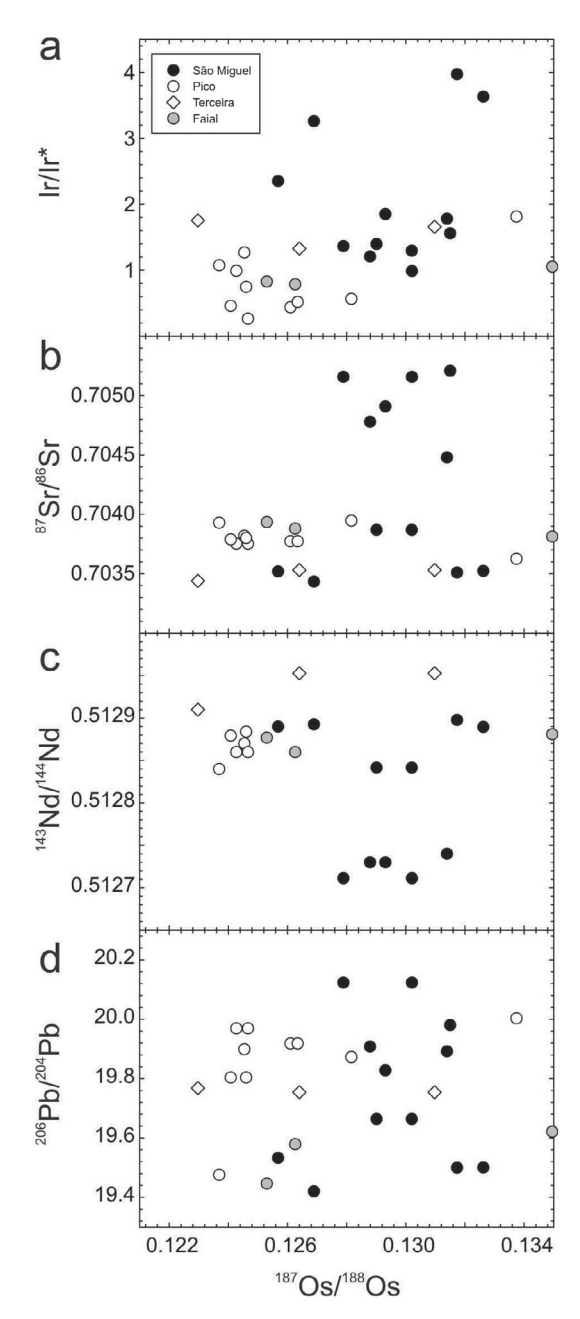


Fig. 8. Plots of $^{187}\text{Os}/^{188}\text{Os}$ versus (a) Ir/Ir*; (b) $^{87}\text{Sr}/^{86}\text{Sr}$; (c) $^{143}\text{Nd}/^{144}\text{Nd}$ and (b) $^{206}\text{Pb}/^{204}\text{Pb}$ for Azores lavas. Uncertainties are smaller than symbols.

between silicate melt and sulfide melt have been determined by several studies. In silicate systems, the HSE span several orders of magnitude ($\sim 10^3 - 10^8$), although the bulk of the studies report values between 10^4 and 5×10^4 (e.g., Peach et al., 1990, 1994; Andrews and Brenan, 2002; Fonseca et al., 2009; Mungall and Brenan, 2014; Day and O'Driscoll, 2019). As a starting point for these models, we assume a mantle source of primitive composition (Day et al., 2017).

In the melt entrainment model, we assume that the entire HSE budget is hosted by sulfides, such that entrain-

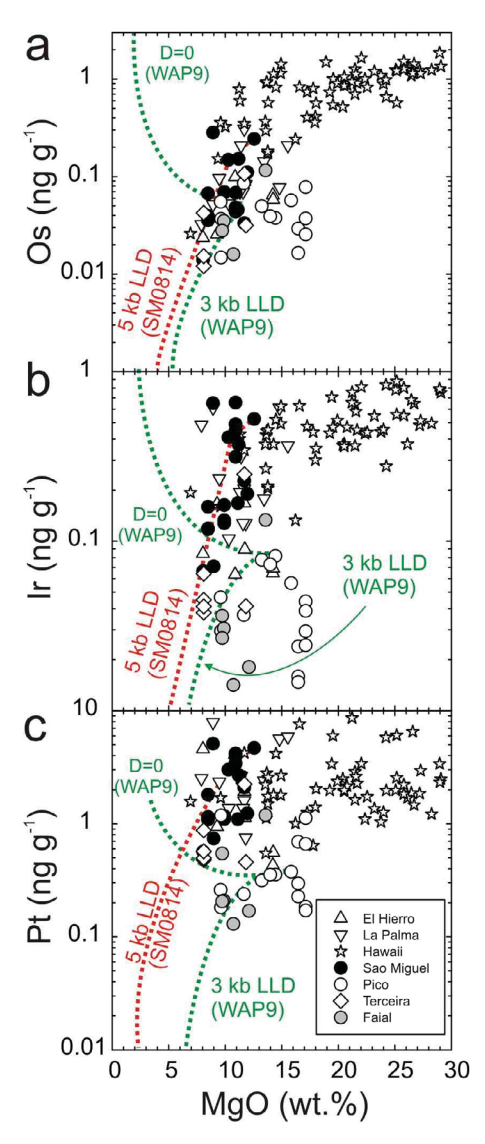


Fig. 9. Variations of MgO (wt.%) versus abundances in ng g⁻¹ (ppb) of (a) Os, (b) Ir, and (c) Pt. Liquid lines of descent (LLD) were estimated for MgO and HSE for parental melts SM0814 for São Miguel lavas and WAP9 for Pico lavas. Crystallization trajectories assuming complete incompatibility (D = 0) of HSEs are also shown. Literature data for the Canary Islands, Hawaii, Azores, and mid-ocean ridges are compiled from Day et al. (2010), Ireland et al. (2009), Widom and Shirey (1996), Schaefer et al. (2002), Bezos et al. (2005), and Gannoun et al. (2007).

ment by melts results only in dilution by a factor proportional to the relative volume proportion of sulfide melt to silicate melt, and that the sum of the sulfide and silicate melt proportion is equal to one. As such, entrainment of sulfide melt will not change HSE ratios. Important variable parameters are the original composition of sulfide in the mantle source and the degrees of melting of sulfide and silicate mantle. We assume $\sim 1.5\%$ melting of silicate mantle in the São Miguel source (Beier et al., 2008) and $\sim 3\%$ melting of silicate mantle in the Pico source (Prytulak and Elliott, 2009; Zanon et al., 2013). Melt compositions for Re are not given because it behaves as a lithophile element

in this system, behaving similarly to K, whereas Re monosulfide solution/sulfide melt partition coefficients reported in Ballhaus et al. (2006) are all >1.8 and give Re concentrations lower than those actually measured in samples.

Mantle sulfide abundance can be estimated from the concentration of the bulk HSE composition within those sulfides to be $\sim 500~\mu g~g^{-1}$ sulfide, which corresponds to $\sim 200~\mu g~g^{-1}$ S, similar to previous estimates of the mantle (cf., McDonough and Sun, 1995; Salters and Stracke, 2004; Mungall and Brenan, 2014). For simplicity, we compare model melts with reasonable examples of parental melt compositions as used in crystallization modeling above, with São Miguel melts represented by SM0814 and Pico melts by WAP9. A model involving a homogeneous mantle source composition cannot explain the differences in parental melt compositions of São Miguel/Terceira and Pico/ Faial lavas (Fig. 10). Namely, the Os-Ir-Ru model abundances for PC-365 SM are too low and Pt-Pd too high compared to SM0814; whereas, while Os-Ir-Ru abundances for PC-365 Pico are similar to WAP9, Pt-Pd are too high. In addition, model melts that provide the closest match to HSE abundances require degrees of sulfide melting (~0.1%) that are too low to explain Azores lava compositions.

In the second model, we use silicate-sulfide melt partitioning in a fractional melting model to estimate parental melt compositions. We use the partition coefficients of Chazey and Neal (2005) (Table S4). Mungall and Brenan (2014) reported sulfide/silicate liquid partition coefficients for the HSE that are one to two orders of magnitude greater than those previously proposed in the literature (e.g., Peach et al., 1990; 1994; Chazey and Neal, 2005). The primary effect of using the higher partition coefficients of Mungall and Brenan (2014) is that the modal abundance of sulfide used to calculate bulk D values must be decreased by a similar factor (i.e., from $\sim 0.1\%$ to $\sim 0.001\%$) to obtain HSE abundances of similar magnitude. Nevertheless, ratios of the partition coefficients for various elements are different from Chazey and Neal (2005), and thus there are also more subtle effects: e.g., using sulfide/silicate liquid HSE partition coefficients of Mungall and Brenan (2014) in our crystallization modeling does not result in a decrease in Pd relative to Pt because D_{Pt}/D_{Pd} is $\sim 25\%$ higher than for Chazey and Neal (2005). Furthermore, recent examination of likely sulfide-melt partitioning for chromitite genesis in mafic-ultramafic intrusions (Day and O'Driscoll, 2019) implies partition coefficients more similar to the empirical values presented by Chazey and Neal (2005). Ultimately, while potentially important if assessing the actual proportion of sulfide fractionated during crystallization, and for "pattern-matching" exercises, using the empirical partition coefficients of Chazey and Neal (2005) does not affect the conclusion that different initial parental melt compositions are required to explain the HSE-MgO systematics for São Miguel versus Pico rocks.

Using: (i) bulk partition coefficients calculated from experimentally derived partition coefficients (either from the compilation of Chazey and Neal, 2005, or Mungall and Brenan, 2014); (ii) a 'normal' mantle HSE composition (Day et al., 2017), and (iii) reasonable estimates of mantle mineralogy does not provide a satisfactory model of melt composition, with respect to either absolute or relative abundances of the HSE (Fig. 10). In contrast, empirically determined estimates of silicate melt-sulfide melt bulk partition coefficients for Hawaiian picrites

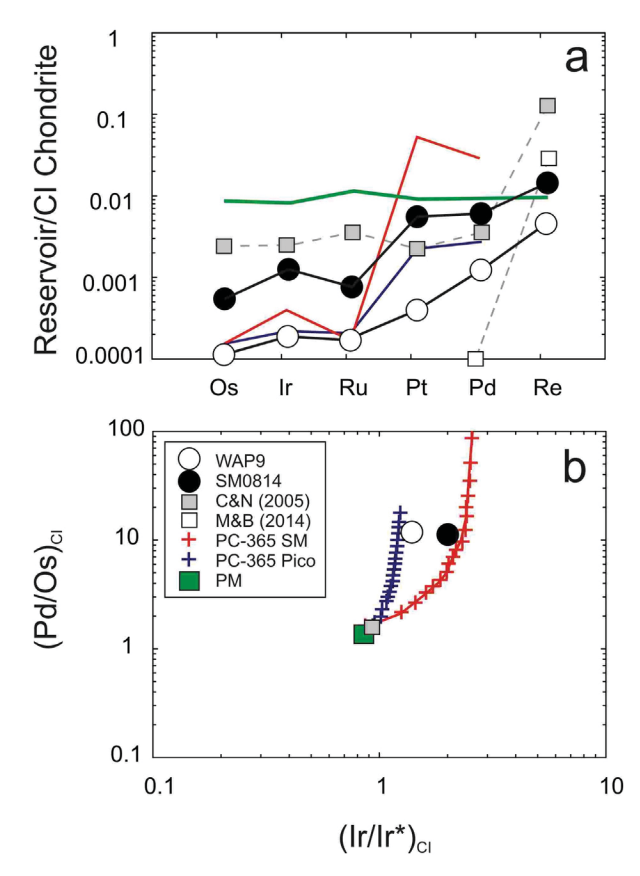


Fig. 10. (a) Chondrite-normalized HSE variations of parental melt proxies SM0814 and WAP9 samples and model fractional melts assuming a primitive mantle source composition (Day et al., 2017) and 1.5% silicate melting for São Miguel and 3% melting for Pico. Model melts calculated using different partition coefficients for the HSE summarized by Chazey and Neal (2005) [C&N (2005)] for silicate solid and melt and for sulfide restite and sulfide melt (Mungall and Brenan, 2014) [M&B (2014)]. Also shown are model melts calculated using the melt entrainment model and mss/sulfide melt partition coefficients reported in Ballhaus et al. (2006) (PC-365 Pico/PC-365 SM). Sulfide melting is 0.1%. (b) Melting trajectories for partial melt entrainment models assuming different partition coefficients illustrating the important effect of Ds on Ir/Ir*.

(Ireland et al., 2009), for Canary alkali basalts (Day, 2013), and for Kohala tholeiites (Jamais et al., 2008), which generally have lower, moderately incompatible D_{Pt} and D_{Pd} , result in steeper patterns more similar to Azorean lavas. A few different sets of mss/sulfide melt partition coefficients reported by Ballhaus et al. (2006) also provide model melts with HSE patterns that are similar to Azorean lavas, particularly with respect to variations in Ir/Ir* (Fig. 10b).

4.4. Evidence for mantle sources with heterogeneous sulfide populations

São Miguel/Terceira lavas are compositionally distinct from Pico/Faial lavas, having:

1. Greater PPGE (Pt + Pd)/IPGE (Os + Ir + Ru) than Pico/Faial lavas.

- 2. Absolute HSE abundances that are roughly a factor of two to five times higher than Pico/Faial lavas, at any given MgO;
- 3. Generally, more radiogenic ¹⁸⁷Os/¹⁸⁸Os (>0.128) than Pico/Faial lavas (<0.126);
- 4. Pronounced ${\rm Ir/Ir_N}^*$ compared to the flat Os-Ir-Ru pattern of Pico/Faial lavas.

The first observation most likely reflects either greater retention of Os, Ir, and Ru in the mantle residue relative to Pt and Pd during partial melting, and/or greater initial mantle source abundances of Pt and Pd relative to Os, Ir, and Ru. All of these features may reflect some combination of differing HSE source abundances and melting conditions (e.g., differing partition coefficients and degrees of sulfide melting) beneath São Miguel compared to Pico, which we explore here.

Studies of mantle peridotites have observed two distinct sulfides populations: M1 - magmatic sulfides enclosed by silicates that have higher HSE abundances, unradiogenic ¹⁸⁷Os/¹⁸⁸Os, and low (Pd/Os)_N, which appear to record primary mantle melt depletion and long-term ingrowth of ¹⁸⁷Os with low Re/Os; M2 - interstitial, metasomatic sulfides with lower HSE abundances and radiogenic ¹⁸⁷Os/¹⁸⁸-Os and high (Pd/Os)_N (Alard et al., 2000; Luguet et al., 2001; Harvey et al., 2011; Burton et al., 2012; Luguet and Reisberg, 2016). Heterogeneous populations of sulfides have not been observed - nor are they anticipated - in volcanic rocks. It follows that distinct HSE patterns and 187-Os/188Os between Pico/Faial and São Miguel/Terceira rocks can be explained by the presence of populations of compositionally distinct sulfides in the mantle. When lavas with similar HSE patterns are grouped (São Miguel/Terceira versus Pico/Faial) and a two-tailed T-test is applied assuming unknown and unequal variances, the null hypothesis that the two-population means are equal can be rejected at the 10% level (p = 0.0854). If we consider only samples with ¹⁸⁷Os/¹⁸⁸Os with the highest precision (< ± 0.001 , 2 σ), the null hypothesis can be rejected at the 5% level (p = 0.0327). Given the limited number of lava samples analyzed from Terceira and Faial, more data may be needed to confirm this observation for these specific islands. Compared to other OIB, Pico and Faial lava ¹⁸⁷-Os/¹⁸⁸Os compositions are relatively unradiogenic, similar to estimates of the depleted mantle (~0.125; e.g., Snow and Reisberg, 1995; Day et al., 2017) or CI chondrites $(\sim 0.126; Day et al., 2016b).$

The Ir enrichments in São Miguel and Terceira lavas, relative to Pico and Faial lavas, cannot be explained by crystallization of major silicate phases, which maintain the relative HSE abundances present in the initial parental melt (e.g., Ir/Os or Pd/Os). Spinel can incorporate Ru (e.g., Day, 2013; Paquet et al., 2019), but spinel is typically not a major phase within Azores lavas. Both Ir enrichments and depletions may result from the accumulation or crystallization of Os-Ru or Ir-rich alloys (e.g., rutheniridosmine, platiniridium) or sulfides (e.g., laurite) from parental magmas with different bulk compositions experiencing different magma reservoir fO₂, fS₂, pressure, and temperature conditions (Brenan and Andrews, 2001). However, there are no clear correlations between MgO and Ir/Ir* or (Pd/Os)_N within São Miguel, Terceira, Pico, or Faial suites, which precludes crystallization of accessory sulfides and alloys as the cause of the observed differences in Ir/Ir* between Pico/Faial and São Miguel/Terceira lava suites.

4.5. Partial melting and mantle source sulfide heterogeneity

A model with two populations of mantle sulfides was used to explore the effects of melting of heterogeneous mantle sulfides, using HSE abundances and ¹⁸⁷Os/¹⁸⁸Os of M1 magmatic and M2 metasomatic sulfides documented in abyssal peridotites (Alard et al., 2005). For the unradiogenic 187Os/188Os M1 sulfide end member, we used 'sulfide g' and for the radiogenic ¹⁸⁷Os/¹⁸⁸Os end-member, we used the M2 generation 'sulfide O' from Kane Fracture Zone (20-24°N Mid-Atlantic Ridge) peridotite KN3-4 (Alard et al., 2005). For each sulfide HSE composition, we calculated the accumulated fractional melt composition as a function of melt fraction using partition coefficients from Ballhaus et al. (2006), detailed in Table S5. The HSE compositions were then determined for all calculated melt fractions independently for each sulfide source. As in the above modeling of a homogeneous mantle source, we assumed that sulfide melt was entrained in melt and that the entire mantle HSE budget was hosted by sulfide (Fig. 11). The same degrees of partial melting of silicate mantle were also used (1.5% for São Miguel, 3% for Pico). Different degree melt fractions of M1 and M2 sulfide melts (e.g., 1% and 30%, respectively) were then mixed in an effort to match measured HSE absolute abundances, Ir/Ir*_N, (Pd/Os)_N, and ¹⁸⁷Os/¹⁸⁸Os compositions in Pico and São Miguel

Although there were numerous successes in modeling the absolute HSE abundances independently of HSE ratios—M2 metasomatic sulfides largely resemble Pico patterns, but at much higher abundances—we were unable to closely match (Pd/Os)_N. In addition, if we closely match the HSE abundances, for example, by mixing $>\sim 80\%$ of M2 sulfide melt ($\sim 90\%$) with 20% or less of M1 sulfide melt, both $^{187}\text{Os}/^{188}\text{Os}$ (~ 0.134) and (Pd/Os)_N (~ 16) are too high (Table S5; Fig. 11).

While successful modeling of parental melt compositions either including ¹⁸⁷Os/¹⁸⁸Os, (Pd/Os)_N, and Ir/Ir_N* or HSE abundances, (Pd/Os)_N, and Ir/Ir_N* is possible, simultaneously modeling HSE abundances, ¹⁸⁷Os/¹⁸⁸Os, (Pd/Os)_N, and Ir/Ir_N* is challenging, regardless of varying the degree of melting for each individual sulfide population, sulfide mantle source abundance, or partition coefficients. These observations indicate that sulfide mantle heterogeneity beneath the Azores is complex—i.e., the heterogeneous sulfide populations in the Pico/Faial mantle source are different than those in the São Miguel/Terceira source—and parental melt HSE compositions are dependent on mantle source sulfide composition. In addition, abyssal peridotite sulfides may not necessarily be representative of sulfides present in the heterogeneous Azorean mantle source, potentially due to greater degrees of depletion in the MORB melting regime represented by abyssal peridotites, and/or differences in HSE abundances and long-term Re/Os ratios of metasomatic sulfides in the Azorean source associated with subduction recycling of diverse lithospheric materials.

In all of the source models presented, the generation of the correct $\rm Ir/Ir_N^*$ anomaly for São Miguel or Pico lavas required the use of partition coefficients from Ballhaus et al. (2006) under reduced conditions (i.e., high atomic Fe-Ni-Cu/S \sim 0.96), where $D_{\rm Os}=3.7,$ $D_{\rm Ir}=1.3,$ $D_{\rm Pt}=0.01,$ and $D_{\rm Pd}=0.03$ (Table S4). Although mantle sulfide HSE composition can have important effects on melt

composition, abyssal peridotite sulfides tend to have Ir/ $Ir_N^* \le 1$ (Luguet et al., 2001; Alard et al., 2005) (Fig. 11), and thus, variations in monosulfide/sulfide melt partitioning appear to be required to generate Ir/Ir_N* > 1. Alternatively, the sulfide populations in the Azorean mantle sources are distinct from abyssal peridotite sulfides. Alloys of the PGE can also potentially control HSE abundances in basaltic magmas and could generate Ir/Ir_N* > 1. However, in S-saturated conditions, typical of the oceanic mantle prior to melting, alloy formation is not reached until relatively high degrees of melting (10-25%, depending on the initial sulfur abundance in the source; Mungall and Brenan, 2014). These conditions are atypical of OIB, and in particular, Azorean, mantle melting conditions (~1-5%, based on previous estimates; Beier et al., 2008; Prytulak and Elliott, 2009; Zanon et al., 2013; Métrich et al., 2014). The low degree of silicate melting, particularly for the São Miguel source, means that sulfide is unlikely to be exhausted and that PGM alloys are unlikely to be stable in the mantle residue (Mungall and Brenan, 2014), and would not be responsible for the Ir anomaly in São Miguel lavas, as was proposed to explain similar Ir anomalies in Fonualei backarc spreading center lavas (Dale et al., 2012).

The fact that Pico/Faial lavas have HSE ratios similar to metasomatic (M2), base-metal sulfides observed in abyssal peridotites (Luguet et al., 2001; Alard et al., 2005) but at lower abundances (Fig. 11), raises the possibility that Pico/Faial lavas may derive from nearly 100% melting of metasomatic sulfides. This is provided that the sulfides have depleted ¹⁸⁷Os/¹⁸⁸Os isotopic compositions (i.e., subchondritic, potentially ancient oceanic depleted upper mantle compositions; e.g., Snow and Reisberg, 1995; Harvey et al., 2006). In contrast, São Miguel/Terceira lavas come from sulfide partial melts with HSE compositions similar to a primitive mantle composition. One possible explanation for this observation is that sulfides are mobile within the silicate mantle such that depleted, residual magmatic sulfides homogenize with metasomatic sulfides (related to enrichment by recycled lithospheric materials) either prior to, or during, partial melting. In either case, these HSEenriched OIB appear to be partial melts of a source similar to the primitive mantle composition.

Model results support a scenario involving melting of a mantle source beneath São Miguel and Terceira that is enriched in metasomatic interstitial sulfides with high (Pd/ $Os)_N$ and $^{187}Os/^{188}Os$, compared to a mantle source beneath Pico and Faial, which has been previously depleted of sulfides and melts to produce OIB with lower (Pd/Os)_N and ¹⁸⁷Os/¹⁸⁸Os. An outcome of this model is that the Pico/Faial mantle source must have overall lower abundances of sulfide compared to the São Miguel/Terceira source. This suggestion might also have implications for the interpretation of Sr-Nd-Pb isotope data, which indicate that the São Miguel mantle source has been refertilized by partial melts or fluids from either ancient basaltic underplate (Elliott et al., 2007), or subduction-recycled seamount volcanic crust (Beier et al., 2007), and with inferences from depleted lithophile incompatible element and Sr-Nd-Pb compositions for substantial melt contributions to Pico and Faial lavas from a relatively depleted, common Azores mantle source (Turner et al., 1997; Elliott et al., 2007; Millet et al., 2009). These observations may also support arguments that the range in ¹⁸⁷Os/¹⁸⁸Os in global OIB can be

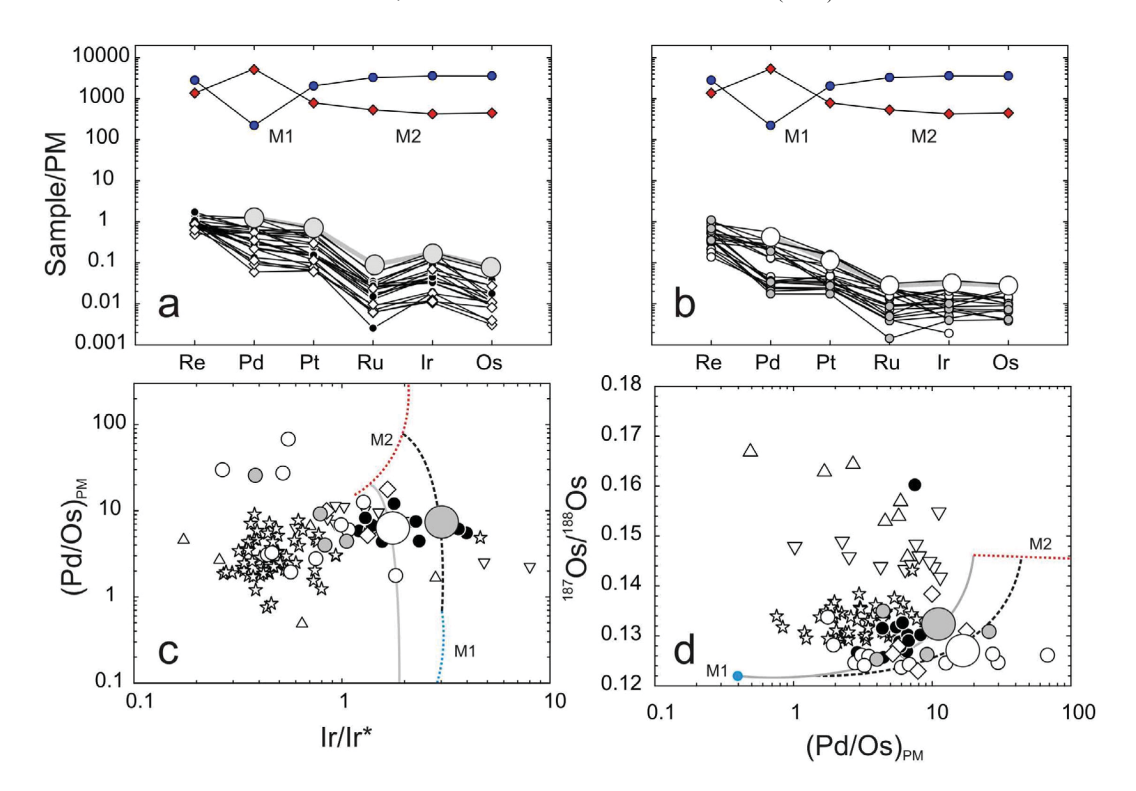


Fig. 11. Model results for melting of heterogeneous sulfides during mantle melting. Chondrite-normalized HSE abundances for (a) São Miguel/Terceira and (b) Pico/Faial lavas (black lines). Also shown are model melts calculated from melting and mixing of melts of heterogeneous sulfide sources composed of M1 and M2 abyssal peridotite sulfides (Alard et al., 2005; M1 = blue circles, and M2 = red diamonds) meant to reproduce a likely primitive parental melt composition. (c) Variations in Ir/Ir* versus (Pd/Os)_{PM} for Azorean, Canarian (Day et al., 2010), and Hawaiian (Ireland et al., 2009) lavas, compared to M1 and M2 abyssal peridotite sulfides. Melt compositions are indicated by dashed black and grey lines, from 0-100% melt increments of the sulfide populations. (d) (Pd/Os)_{PM} versus ¹⁸⁷Os/¹⁸⁸Os. Note that when Pico lava HSE abundances are reproduced well, both (Pd/Os)_{PM} and ¹⁸⁷Os/¹⁸⁸Os are unrealistically high. (For interpretation of the references to color in this figure legend, the reader is referred to the web version of this article.)

explained by sulfide metasomatism by pyroxenite/peridotite partial melts associated with recycling of lithospheric materials (Luguet et al., 2008). The results from the Azores are also consistent with evidence from OIB magmatic products from Réunion Island that indicate that mantle domains are preserved with distinct sulfide, HSE and siderophile element inventories (Peters et al., 2016).

4.6. Global mantle ¹⁸⁷Os/¹⁸⁸Os and HSE heterogeneity

Osmium isotopes and the HSE do not appear to record mantle enrichment and depletion events in the same way as lithophile radiogenic isotopes and incompatible trace elements in the Azores. If Sr, Nd, Hf, and Pb isotopic enrichment is due, at least partly, to recycled oceanic crust or metasomatism (e.g., White and Hofmann, 1982), and ¹⁸⁷-Os/¹⁸⁸Os enrichment to associated sulfide metasomatism in OIB mantle sources, then it is unsurprising that lithophile and siderophile isotope compositions are decoupled (Fig. 8), since sulfide is more mobile than silicate. Decoupling of Os and Pb isotopes in Azorean lavas and most OIB is further supported by hosting of Os in sulfide and Pb in silicate in abyssal peridotites (Burton et al., 2012; Warren and Shirey, 2012). Siderophile Os and lithophile Pb parent-daughter element fractionation may record dis-

tinct processes during the same geological event (e.g., oceanic crustal recycling).

In the case of São Miguel, the enriched component present in some of the geographically eastern-most located lavas is not exclusively associated with the Os isotope and HSE characteristics of São Miguel and Terceira volcanic rocks. Instead, it appears that a wide-spread source exists beneath this region where melting of disseminated, relatively young metasomatic sulfides produces melt with radiogenic ¹⁸⁷Os/¹⁸⁸Os but relatively low Os abundances. This melt may be diluted to some extent by melting of higher Os abundance, less radiogenic ¹⁸⁷Os/¹⁸⁸Os peridotitehosted sulfides. However, the lithophile elemental and isotopic (e.g., Pb) signature would be dominated by the silicate melts of the more productive mafic lithology over those of incompatible element-poor peridotite (Pertermann and Hirschmann, 2003; Prytulak and Elliott, 2009; Waters et al., 2011). In regions of greater melt depletion like the source for Pico lavas, more depleted sulfides (whether metasomatic base metal sulfides or silicate-enclosed primary monosulfides) with less radiogenic ¹⁸⁷Os/¹⁸⁸Os dominate the HSE and ¹⁸⁷Os/¹⁸⁸Os budget during partial melting, but radiogenic Pb from more abundant silicate melts will dilute any unradiogenic Pb derived from sulfides (Burton et al., 2012; Warren and Shirey, 2012).

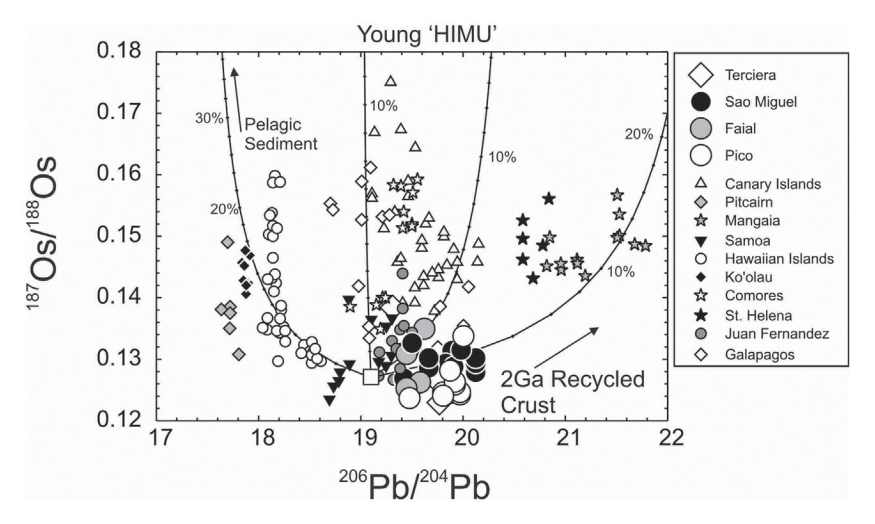


Fig. 12. Plot of ²⁰⁶Pb/²⁰⁴Pb versus ¹⁸⁷Os/¹⁸⁸Os for OIB with >0.05 pg g⁻¹ Os. Shown are mixing curves between a common ('C') mantle component (unfilled square, with Pb defined by Hanan and Graham, 1996, and Os from Day et al., 2010) and 2 Ga recycled oceanic crust, pelagic sediment and material conforming to 'layer 2' and 'layer 3' recycled oceanic crust and lithosphere. Canary Island lavas can be modeled as mixtures of 'C' and <5–10% of HIMU-like pyroxenite-rich mantle with distinct proportions of 'layer 2' or 'layer 3' materials (Day et al., 2009). Hawai'ian post-erosional lavas can also be explained as pyroxenite-peridotite mixtures (Lassiter et al., 2000). Figure adapted from Day (2013), with updated data for Galapagos and the Juan Fernandez Islands from Gibson et al. (2016) and Paquet et al. (2019), respectively.

This effect can be illustrated in a plot of ²⁰⁶Pb/²⁰⁴Pb versus ¹⁸⁷Os/¹⁸⁸Os, where mixing of a peridotitic source with old (>2 Ga) recycled crust in the case of the Azores (cf., Elliott et al., 2007) produces a strongly hyperbolic mixing curve (Fig. 12). Limited additions of radiogenic Pb (whether solid source mixing or melt mixing) from the recycled crustal source would result in lavas with more radiogenic Pb. However, although the Os from recycled sulfides would also be highly radiogenic, the low Os abundances would be overwhelmed by the high abundances of unradiogenic sulfides in depleted peridotite mantle.

Lavas associated with different islands within the Azorean (Pico/Faial versus São Miguel/Terceira), Canarian (La Palma versus El Hierro) (Day et al., 2010), and Hawaiian (Mauna Kea, Mauna Loa versus Loihi; Ireland et al., 2009) archipelagos can be grouped on the basis of HSE abundances: lavas with low (Pd/Os)_N and relatively unradiogenic ¹⁸⁷Os/¹⁸⁸Os, or lavas with high (Pd/Os)_N and ¹⁸⁷-Os/¹⁸⁸Os (Fig. 13). For Hawaii, we report lavas from volcanoes with ²⁰⁸Pb*/²⁰⁶Pb* akin to Kea (depleted) or Loa (enriched) compositions from Abouchami et al. (2005). Although there are clear geographic distinctions in relative and absolute abundances of the HSE among Azorean islands, lavas from the Canaries and Hawaii do not always display the same clear inter-island HSE compositional differences. For example, lavas from El Hierro and La Palma in the Canaries display both types of patterns (Day et al., 2010), although Canaries Type I lavas, which are similar to São Miguel compositions, are dominantly from La Palma (Fig. 13). For the Hawaiian archipelago, available HSE data appears to fall into two compositional groups; Type I, which are Kea trend dominant and Type II, which are Loa trend dominant. Loihi lavas are all Type I, and ²⁰⁸Pb*/²⁰⁶Pb* compositions straddle the Loa/Kea trend compositions. Further work is needed to examine sulfide mantle source heterogeneity in other OIB in more detail, but HSE abundances appear distinct among these three island chains examined, with Hawaiian HSE patterns

having the highest absolute abundances, and Azorean lavas having the lowest absolute abundances, reflecting different extents of partial melting.

"Type II" Hawaiian picrites, as defined by Ireland et al. (2009) (our Type I), have high (Pd/Os)_N, but closely resemble the depleted suites from the Azores (Pico) and Canaries (La Palma) that exhibit small Ir/Ir* anomalies, despite having higher overall HSE abundances. Hawaiian lavas defined by Ireland et al. (2009) as thier Type I (Hawaii Type II in Fig. 13), which primarily include Mauna Kea, Hualalai, and Koolau lavas, have lower (Pd/Os)_N, and have HSE relative abundances similar to primitive mantle—including distinct Ir/Ir* < 1—but at lower absolute abundances. These observations suggest that both locally and regionally heterogeneous sulfide mineralogy with distinct HSE abundances has an important controlling effect on the HSE composition of mantle-derived melts. Equally, melting controls, such as mantle potential temperature or lithospheric thickness may also play roles in the determination of HSE signatures in OIB from distinct mantle sulfide populations. For example, the greater lithospheric thickness underneath São Miguel and Terceira relative to Pico and Faial may have led to sampling of different sulfide populations. Ultimately, the HSE compositions of OIB suggest sulfide compositions in Earth's mantle are globally variable and more heterogeneous than previously thought.

5. CONCLUSIONS

New major-element, trace-element, and highly siderophile element abundances, and Sr, Nd, Hf, Pb, and Os isotope compositions are reported for primitive and cumulate basalts from São Miguel, Terceira, Pico, and Faial islands in the Azores archipelago to evaluate the relationships among siderophile and lithophile elemental and radiogenic isotope compositions. Variations in HSE abundances in Azorean lavas from individual islands result from first-

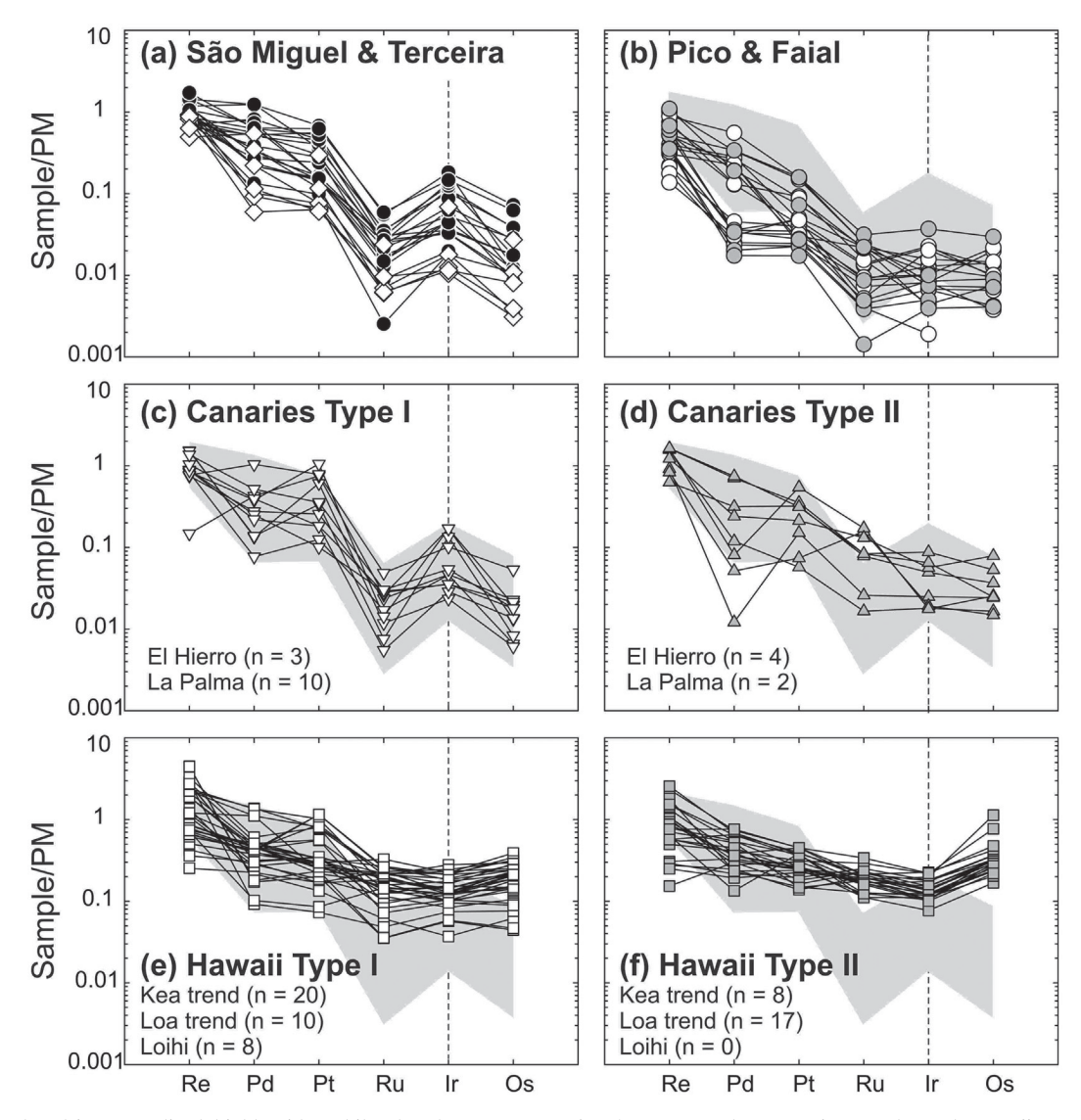


Fig. 13. Chondrite-normalized highly siderophile abundance patterns for Azorean (a, b), Canarian (c, d), and Hawaiian (e, f) lavas, illustrating the distinctive compositional variations that exist within and among ocean island basalt chains. Gray field shows range of Sāo Miguel and Terceira lavas. Numbers of samples for El Hierro and La Palma are shown. For Hawaii, samples are separated based on the reported ²⁰⁸Pb*/²⁰⁶Pb* of their source volcano (from Abouchami et al., 2005). See text for discussion. Data for Canary and Hawaiian lavas are from Day et al. (2010) and Ireland et al. (2009), respectively.

order control by sulfide crystallization, but distinct ¹⁸⁷Os/¹⁸⁸Os and HSE inter-island variations between Pico/Faial and São Miguel/Terceira can only be attributed to partial melting of a heterogeneous mantle source. Lavas from Pico and Faial are more depleted in HSE abundances due to melting of a long-term depleted sulfide source with unradiogenic ¹⁸⁷Os/¹⁸⁸Os (<0.126), whereas lavas from São Miguel and Terceira are more enriched, owing to more recent additions of metasomatic sulfides with more radiogenic ¹⁸⁷Os/¹⁸⁸Os (>0.128). Sulfides in the São Miguel mantle source may result from metasomatism associated with subduction recycling of oceanic lithosphere, which has been proposed to explain the lithophile elemental and radiogenic isotope systematics of São Miguel lavas. The ¹⁸⁷Os/¹⁸⁸Os ratios and the HSE are decoupled from lithophile isotope

compositions and Pb isotope compositions in particular, which can be explained if Os (and the HSE) is hosted by sulfide minerals whereas Pb is hosted by silicate minerals in the mantle. Thus, HSE respond to sulfide melting and remobilization, whereas lithophile elements respond to silicate melting. The HSE compositional variations among global OIB suggest that while distinct mantle domains are represented by heterogeneous sulfide mineralogy comprising common metasomatic (enriched) and magmatic (depleted) sulfides, these sulfide populations are distinct beneath individual ocean island chains due to their origin in different lithospheric materials (e.g., oceanic crust versus pelagic sediments). The HSE compositions of OIB suggest sulfide compositions in Earth's mantle are globally variable and heterogeneous.

Declaration of Competing Interest

The authors declare no conflicts of interest.

ACKNOWLEDGEMENTS

We thank José Pacheco for assisting with fieldwork in the Azores. B. Schaefer and S. Turner are thanked for provision of the P5, F/CA 6 and MAR samples. The constructive comments of Christoph Beier, Sally Gibson and two anonymous reviewers, as well as from the A.E., Julie Prytulak, are greatly appreciated. Funding for this study was provided by the National Geographic Society, National Science Foundation grants NSF-EAR 1116089, 1447130 and 1918322 to J.M.D.D, NSF-OCE 0079943 to B.B.H., and a Scripps Postdoctoral Scholarship to C.L.W.

APPENDIX A. SUPPLEMENTARY MATERIAL

Supplementary data to this article can be found online at https://doi.org/10.1016/j.gca.2019.10.012.

REFERENCES

- Abouchami W., Hofmann A. W., Galer S. J. G., Frey F. A., Eisele J. and Feigenson M. (2005) Lead isotopes reveal bilateral asymmetry and vertical continuity in the Hawaiian mantle plume. *Nature* **434**, 851–856.
- Alard O., Griffin W. L., Lorand J. P., Jackson S. E. and O'Reilly S. Y. (2000) Non-chondritic distribution of the highly siderophile elements in mantle sulfides. *Nature* 407, 891–894.
- Alard O., Luguet A., Pearson N. J., Griffin W. L., Lorand J.-P., Gannoun A., Burton K. W. and O'Reilly S. Y. (2005) *In situ* Os isotopes in abyssal peridotites bridge the isotopic gap between MORBs and their source mantle. *Nature* 436, 1005–1008.
- Andrews D. R. and Brenan J. M. (2002) Phase-equilibrium constraints on the magmatic origin of laurite+ Ru-Os-Ir alloy. *Canadian Mineral.* 40, 1705–1716.
- Ballhaus C., Bockrath C., Wohlgemuth-Ueberwasser C., Laurenz V. and Berndt J. (2006) Fractionation of the noble metals by physical processes. *Contrib. Miner. Petrol.* 152(6), 667–684.
- Barnes S.-J., Naldrett A. J. and Gorton M. P. (1985) The origin of the fractionation of platinum-group elements in terrestrial magmas. *Chem. Geol.* 53, 302–323.
- Béguelin P., Bizimis M., Beier C. and Turner S. (2017) Rift-plume interaction reveals multiple generations of recycled oceanic crust in Azores lavas. *Geochim. Cosmochim. Acta* 218, 132–152.
- Beier C., Haase K. M. and Hansteen T. H. (2006) Magma evolution of the Sete Cidades volcano, São Miguel, Azores. *J. Petrol.* 47, 1375–1411.
- Beier C., Stracke A. and Haase K. M. (2007) The peculiar geochemical signatures of São Miguel (Azores) lavas: metasomatised or recycled mantle sources? *Earth Planet. Sci. Lett.* 259 (1), 186–199.
- Beier C., Haase K. M., Abouchami W., Krienitz M. S. and Hauff F. (2008) Magma genesis by rifting of oceanic lithosphere above anomalous mantle: Terceira Rift, Azores. *Geochem., Geophys., Geosyst.* 9(12). https://doi.org/10.1029/2008GC002112.
- Beier C., Turner S., Plank T. and White W. (2010) A preliminary assessment of the symmetry of source composition and melting dynamics across the Azores plume. *Geochem. Geophys. Geosyst.* 11(2).

- Beier C., Haase K. M. and Turner S. P. (2012) Conditions of melting beneath the Azores. *Lithos* 144, 1–11.
- Bezos A., Lorand J.-P., Humler E. and Gros M. (2005) Platinum-group element systematics in Mid-Oceanic Ridge basaltic glasses from the Pacific, Atlantic, and Indian Oceans. *Geochim. Cosmochim. Acta* **69**(10), 2613–2627.
- Birck J.-L., Roy Barman M. and Capmas F. (1997) Re-Os isotopic measurements at the femtomole level in natural samples. *Geostandards Newsletter* **21**(1), 19–27.
- Blichert-Toft J. and Albarède F. (1997) The Lu-Hf isotope geochemistry of chondrites and the evolution of the mantle-crust system. *Earth Planet. Sci. Lett.* **148**(1), 243–258.
- Bockrath C., Ballhaus C. and Holzheid A. (2004) Fractionation of the platinum-group elements during mantle melting. *Science* 305, 1951–1953.
- Boyd F. R. and Mertzman S. A. (1987) Composition and structure of the Kaapvaal lithosphere, southern Africa. *Magmatic Proces.: Physicochem. Princ.* 1, 13–24.
- Brandon A. D., Norman M. D., Walker R. J. and Morgan J. W. (1999) ¹⁸⁶Os¹⁸⁷Os systematics of Hawaiian picrites. *Earth Planet. Sci. Lett.* **174**(1), 25–42.
- Brandon A. D., Graham D. W., Waight T. and Gautason B. (2007) ¹⁸⁶Os and ¹⁸⁷Os enrichments and high-³He/⁴He sources in the Earth's mantle: evidence from Icelandic picrites. *Geochim. Cosmochim. Acta* **71**, 4570–4591.
- Brenan J. M. and Andrews D. (2001) High-temperature stability of laurite and Ru-Os-Ir alloy and their role in PGE fractionation in mafic magmas. *Canadian Mineral.* 39(2), 341–360.
- Brenan J. M., Finnigan C. F., McDonough W. F. and Homolova V. (2012) Experimental constraints on the partitioning of Ru, Rh, Ir, Pt and Pd between chromite and silicate melt: the importance of ferric iron. *Chem. Geol.* 302, 16–32.
- Brenan J. M., Bennett N. R. and Zajacz Z. (2016) Experimental results on fractionation of the highly siderophile elements (HSE) at variable pressures and temperatures during planetary and magmatic differentiation. *Rev. Mineral. Geochem.* 81, 1–87.
- Burton K. W., Cenki-Tok B., Mokadem F., Harvey J., Gannoun A., Alard O. and Parkinson I. J. (2012) Unradiogenic lead in the Earth's upper mantle. *Nat. Geosci.* **5**, 570–573.
- Chazey W. J. and Neal C. R. (2005) Platinum-group element constraints on source composition and magma evolution of the Kerguelen Plateau using basalts from ODP Leg 183. *Geochim. Cosmochim. Acta* 69(19), 4685–4701.
- Class C., Goldstein S. L. and Shirey S. B. (2009) Osmium isotopes in Grand Comore lavas: a new extreme among a spectrum of EM-type mantle endmembers. *Earth Planet. Sci. Lett.* 284, 219– 227
- Cohen A. S. and Waters F. G. (1996) Separation of osmium from geological materials by solvent extraction for analysis by thermal ionization mass spectrometry. *Anal. Chim. Acta* **332** (2–3), 269–275.
- Dale C. W., Macpherson C. G., Pearson D. G., Hammond S. J. and Arculus R. J. (2012) Inter-element fractionation of highly siderophile elements in the Tonga Arc due to flux melting of a depleted source. *Geochim. Cosmochim. Acta* 89, 202–225.
- Day J. M. D. (2013) Hotspot volcanism and highly siderophile elements. *Chem. Geol.* **341**, 50–74.
- Day J. M. D. and O'Driscoll B. (2019) Ancient high Pt/Os crustal contaminants can explain radiogenic ¹⁸⁶Os in intraplate magmas. *Earth Planet. Sci. Lett.* 519, 101–108.
- Day J. M. D., Pearson D. G., Macpherson C. G., Lowry D. and Carracedo J. C. (2009) Pyroxenite-rich mantle formed by recycled oceanic lithosphere: oxygen-osmium isotope evidence from Canary Island lavas. *Geology* 37(6), 555–558.

- Day J. M. D., Pearson D. G., Macpherson C. G., Lowry D. and Carracedo J.-C. (2010) Evidence for distinct proportions of subducted oceanic crust and lithosphere in HIMU-type mantle beneath El Hierro and La Palma, Canary Islands. *Geochim. Cosmochim. Acta* 74, 6565–6589.
- Day J. M. D., Peters B. J. and Janney P. E. (2014) Oxygen isotope systematics of South African olivine melilitites and implications for HIMU mantle reservoirs. *Lithos* **202–203**, 76–84.
- Day J. M. D., Waters C. L., Schaefer B. F., Walker R. J. and Turner S. (2016a) Use of hydrofluoric acid desilicification in the determination of highly siderophile element abundances and Re-Pt-Os isotope systematics in mafic-ultramafic rocks. *Geo-stand. Geoanal. Res.* 40, 49–65.
- Day J. M. D., Walker R. J. and Brandon A. D. (2016b) Highly siderophile elements in Earth, the Moon, Mars and asteroids. *Rev. Mineral. Geochem.* 81, 161–238.
- Day J. M. D., Walker R. J. and Warren J. M. (2017) ¹⁸⁶Os-¹⁸⁷Os and highly siderophile element abundance systematics of the mantle revealed by abyssal peridotites and Os-rich alloys. *Geochim. Cosmochim. Acta* 200, 232–254.
- Eisele J., Sharma M., Galer S. J. G., Blichert-Toft J., Devey C. W. and Hofmann A. W. (2002) The role of sediment recycling in EM-1 inferred from Os, Pb, Hf, Nd, Sr isotope and trace element systematics of the Pitcairn hotspot. *Earth Planet. Sci. Lett.* **196**, 197–212.
- Elliott T., Blichert-Toft J., Heumann A., Koetsier G. and Forjaz V. (2007) The origin of enriched mantle beneath São Miguel, Azores. Geochim. Cosmochim. Acta 71(1), 219–240.
- Flower M. F. J., Schmincke H. U. and Bowman H. (1976) Rare earth and other trace elements in historic Azorean lavas. *J. Volcanol. Geoth. Res.* 1, 127–147.
- Fonseca R. O., Campbell I. H., O'Neill H. S. C. and Allen C. M. (2009) Solubility of Pt in sulphide mattes: implications for the genesis of PGE-rich horizons in layered intrusions. *Geochim. Cosmochim. Acta* 73, 5764–5777.
- França Z., Lago San José M., Nunes J. C., Galé C., Forjaz V. H., Pueyo Anchuela Ó. and Arranz E. (2006) Geochemistry of alkaline basalts of Corvo Island (Azores, Portugal): preliminary data. *Geogaceta* **40**, 87–90.
- Gannoun A., Burton K. W., Parkinson I. J., Alard O., Schiano P. and Thomas L. E. (2007) The scale and origin of the osmium isotope variations in mid-ocean ridge basalts. *Earth Planet. Sci. Lett.* 209, 541–556.
- Gannoun A., Burton K. W., Day J. M. D., Harvey J., Schiano P. and Parkinson I. (2016) Highly siderophile element and Os Isotope Systematics of volcanic rocks at divergent and convergent plate boundaries and in intraplate settings. *Rev. Mineral. Geochem.* 81, 651–724.
- Gast P. W., Tilton G. R. and Hedge C. (1964) Isotopic composition of lead and strontium from Ascension and Gough Islands. *Science* **145**(3637), 1181–1185.
- Genske F. S., Turner S. P., Beier C., Chu M. F., Tonarini S., Pearson N. J. and Haase K. M. (2014) Lithium and boron isotope systematics in lavas from the Azores islands reveal crustal assimilation. *Chem. Geol.* 373, 27–36.
- Genske F. S., Beier C., Stracke A., Turner S. P., Pearson N. J., Hauff F., Schaefer B. F. and Haase K. M. (2016) Comparing the nature of the western and eastern Azores mantle. *Geochim. Cosmochim. Acta* 172, 76–92.
- Ghiorso M. S. and Sack R. O. (1995) Chemical mass transfer in magmatic processes IV. A revised and internally consistent thermodynamic model for the interpolation and extrapolation of liquid-solid equilibria in magmatic systems at elevated temperatures and pressures. *Contrib. Miner. Petrol.* 119, 197– 212.

- Gibson S. A., Dale C. W., Geist D. J., Day J. A., Brügmann G. and Harpp K. S. (2016) The influence of melt flux and crustal processing on Re–Os isotope systematics of ocean island basalts: Constraints from Galápagos. *Earth Planet. Sci. Lett.* 449, 345–359.
- Hanan B. B. and Schilling J.-G. (1989) Easter microplate evolution—Pb isotope evidence. *J. Geophys. Res.: Solid Earth Planets* **94**(B6), 7432–7448.
- Hanan B. B. and Graham D. W. (1996) Lead and helium isotope evidence from oceanic basalts for a common deep source of mantle plumes. *Science* 272, 991–995.
- Harvey J., Gannoun A., Burton K. W., Rogers N. W., Alard O. and Parkinson I. J. (2006) Ancient melt extraction from the oceanic upper mantle revealed by Re-Os isotopes in abyssal peridotites from the Mid-Atlantic ridge. *Earth Planet. Sci. Lett.* 244, 606–621.
- Harvey J., Dale C. W., Gannoun A. and Burton K. W. (2011) Osmium mass balance in peridotite and the effects of mantlederived sulfides on basalt petrogenesis. *Geochim. Cosmochim.* Acta 75, 5574–5596.
- Hauri E. H. and Hart S. R. (1993) Re-Os isotope systematics of HIMU and EMII oceanic island basalts from the South Pacific Ocean. *Earth Planet. Sci. Lett.* 114, 353–371.
- Hawkesworth C. J., Norry M. J., Roddick J. C. and Vollmer R. (1979) 143Nd/144Nd and 87Sr/86Sr ratios from the Azores and their significance in LIL-element enriched mantle. *Nature* **280**, 28–31
- Herzberg C. and Asimow P. D. (2015) PRIMELT 3 MEGA. XLSM software for primary magma calculation: peridotite primary magma MgO contents from the liquidus to the solidus. *Geochem. Geophys. Geosyst.* 16, 563–578.
- Ireland T. J., Walker R. J. and Garcia M. O. (2009) Highly siderophile element and ¹⁸⁷Os isotope systematics of Hawaiian picrites: implications for parental melt composition and source heterogeneity. *Chem. Geol.* 260(1), 112–128.
- Jamais M., Lassiter J. C. and Brügmann G. (2008) PGE and Osisotopic variations in lavas from Kohala Volcano, Hawaii: constraints on PGE behaviour and melt/crust interaction. *Chem. Geol.* 250, 16–28.
- Lassiter J. C. and Hauri E. H. (1998) Osmium-isotope variations in Hawaiian lavas: evidence for recycled oceanic lithosphere in the Hawaiian plume. *Earth Planet. Sci. Lett.* **164**, 483–496.
- Lassiter J. C., Hauri E. H., Reiners P. W. and Garcia M. O. (2000) Generation of Hawaiian post-erosional lavas by melting of a mixed lherzolite/pyroxenite source. *Earth Planet. Sci. Lett.* 178, 269–284.
- Lassiter J. C., Blichert-Toft J., Hauri E. H. and Barsczus H. G. (2003) Isotope and trace element variations in lavas from Raivavae and Rapa, Cook-Austral Islands: constraints on the nature of HIMU- and EM-mantle and the origin of mid-plate volcanism in French Polynesia. *Chem. Geol.* 202, 115–138.
- Lorand J. P. and Luguet A. (2016) Chalcophile and siderophile elements in mantle rocks: trace elements controlled by trace minerals. Rev. Mineral. Geochem. 81, 441–488.
- Luguet A. and Reisberg L. (2016) Highly siderophile element and ¹⁸⁷Os signatures in non-cratonic basalt-hosted peridotite xeno-liths: unravelling the origin and evolution of the post-Archean lithospheric mantle. *Rev. Mineral. Geochem.* **81**, 305–367.
- Luguet A., Alard O., Lorand J. P., Pearson N. J., Ryan C. and O'Reilly S. Y. (2001) Laser-ablation microprobe (LAM)-ICPMS unravels the highly siderophile element geochemistry of the oceanic mantle. *Earth Planet. Sci. Lett.* 189, 285–294.
- Luguet A., Pearson D. G., Nowell G. M., Dreher S. T., Coggon J. A., Spetsius Z. V. and Parman S. W. (2008) Enriched Pt-Re-Os

- isotope systematics in plume lavas explained by metasomatic sulfides. *Science* **319**, 453–456.
- Madureira P., Moreira M., Mata J. and Allègre C. J. (2005) Primitive neon isotopes in Terceira Island (Azores archipelago). *Earth Planet. Sci. Lett.* **233**(3), 429–440.
- Madureira P., Mata J., Mattielli N., Queiroz G. and Silva P. (2011) Mantle source heterogeneity, magma generation and magmatic evolution at Terceira Island (Azores archipelago): constraints from elemental and isotopic (Sr, Nd, Hf, and Pb) data. *Lithos* 126, 402–418.
- McDonough W. F. and Sun S. S. (1995) The composition of the Earth. *Chem. Geol.* **120**, 223–253.
- Métrich N., Zanon V., Créon L., Hildenbrand A., Moreira M. and Marques F. O. (2014) Is the "Azores hotspot" a wet spot? Insights from geochemistry of fluid and melt inclusions in olivines of Pico basalts. J. Petrol. 55, 377–393.
- Millet M. A., Doucelance R., Baker J. A. and Schiano P. (2009) Reconsidering the origins of isotopic variations in Ocean Island Basalts: insights from fine-scale study of S\u00e4o Jorge Island, Azores archipelago. Chem. Geol. 265(3), 289–302.
- Moreira M., Doucelance R., Kurz M. D., Dupré B. and Allègre C. J. (1999) Helium and lead isotope geochemistry of the Azores Archipelago. *Earth Planet. Sci. Lett.* **169**(1), 189–205.
- Mungall J. E. and Brenan J. M. (2014) Partitioning of platinumgroup elements and Au between sulfide liquid and basalt and the origins of mantle-crust fractionation of the chalcophile elements. Geochim. Cosmochim. Acta 125, 265–289.
- Nier A. O. (1950) A redetermination of the relative abundances of the isotopes of carbon, nitrogen, oxygen, argon, and potassium. *Phys. Rev.* 77(6), 789–793.
- Paquet M., Day J. M. D. and Castillo P. R. (2019) Osmium isotope evidence for a heterogeneous ³He/⁴He mantle plume beneath the Juan Fernandez Islands. *Geochim. Cosmochim. Acta* **261**, 1–19
- Peach C. L., Mathez E. A. and Keays R. R. (1990) Sulphide meltsilicate melt distribution coefficients for noble metals and other chalcophile elements as deduced from MORB: Implications for partial melting. *Geochim. Cosmochim. Acta* 54, 3379–3389.
- Peach C. L., Mathez E. A., Keays R. R. and Reeves S. J. (1994) Experimentally determined sulfide silicate-melt partition coefficients for iridium and palladium. *Chem. Geol.* 117, 361–377.
- Pegram W. J. and Allègre C. J. (1992) Osmium isotopic compositions from oceanic basalts. *Earth Planet. Sci. Lett.* **111**, 59–68.
- Pertermann M. and Hirschmann M. M. (2003) Partial melting experiments on a MORB-like pyroxenite between 2 and 3 GPa: constraints on the presence of pyroxenite in basalt source regions from solidus location and melting rate. *J. Geophys. Res. Solid Earth* 108(B2).
- Peters B. J., Day J. M. D. and Taylor L. A. (2016) Early mantle heterogeneities in the Réunion hotspot source inferred from highly siderophile elements in cumulate xenoliths. *Earth Planet. Sci. Lett.* 448, 150–160.
- Prytulak J. and Elliott T. (2009) Determining melt productivity of mantle sources from ²³⁸U–^{230Th} and ²³⁵U–²³¹Pa disequilibria; an example from Pico Island, Azores. *Geochim. Cosmochim. Acta* **73**, 2103–2122.
- Prytulak J., Avanzinelli R., Koetsier G., Kreissig K., Beier C. and Elliott T. (2014) Melting versus contamination effects on ²³⁸-U-²³⁰Th-²²⁶Ra and ²³⁵U-²³¹Pa disequilibria in lavas from São Miguel, Azores. *Chem. Geol.* **381**, 94–109.
- Puchtel I. S. and Humayun M. (2001) Platinum group element fractionation in a komatiitic basalt lava lake. *Geochim. Cosmochim. Acta* 65(17), 2979–2993.
- Rehkämper M., Halliday A. N., Fitton J. G., Lee D.-C., Wieneke M. and Arndt N. T. (1999) Ir, Ru, Pt and Pd in basalts and

- komatiites: new constraints for the geochemical behaviour of the platinum-group elements in the mantle. *Geochim. Cosmochim. Acta* **63**, 3915–3934.
- Reisberg L., Zindler A., Marcantonio F., White W., Wymna D. and Weaver B. (1993) Os isotope systematics in ocean island basalts. *Earth Planet. Sci. Lett.* 120(3–4), 149–167.
- Rooney T. O., Hanan B. B., Graham D. W., Furman T., Blichert-Toft J. and Schilling J.-G. (2012) Upper mantle pollution during Afar plume-continental rift interaction. *J. Petrol.* 53, 365–389.
- Salters V. J. and Stracke A. (2004) Composition of the depleted mantle. *Geochem. Geophys. Geosyst.* **5**(5).
- Schaefer B. F., Turner S., Parkinson I., Rogers N. and Hawkesworth C. (2002) Evidence for recycled Archaean oceanic mantle lithosphere in the Azores plume. *Nature* 420(6913), 304–307.
- Schiano P., Burton K. W., Dupre B., Birck J.-L., Guille G. and Allegre C.-J. (2001) Correlated Os-Pb-Nd-Sr isotopes in the Austral-Cook chain basalts: the nature of mantle components in plume sources. *Earth Planet. Sci. Lett.* 186, 527–537.
- Self S. and Gunn B. M. (1976) Petrology, volume and age relations of alkaline and saturated peralkaline volcanics from Terceira, Azores. *Contrib. Miner. Petrol.* **54**, 293–313.
- Shirey S. B. and Walker R. J. (1998) The Re-Os isotope system in cosmochemistry and high temperature geochemistry. *Annu. Rev. Earth Planet. Sci.* **26**, 423–500.
- Snow J. E. and Reisberg L. (1995) Os isotopic systematics of the MORB mantle: results from altered abyssal peridotites. *Earth Planet. Sci. Lett.* 133(3), 411–421.
- Todt R. A. (1996) Evaluation of a ²⁰²Pb-²⁰⁵Pb double spike for high-precision lead isotope analysis. In *Earth processes: reading* the isotopic code: geophysical monograph (eds. A. Basu and S. Hart). American Geophysical Union, Washington, D.C., pp. 429–437.
- Turner S., Hawkesworth C., Rogers N. and King P. (1997) U-Th isotope disequilibria and ocean island basalt generation in the Azores. *Chem. Geol.* **139**(1), 145–164.
- Warren J. M. and Shirey S. B. (2012) Lead and osmium isotopic constraints on the oceanic mantle from single abyssal peridotite sulfides. *Earth Planet. Sci. Lett.* 359–360, 279–293.
- Waters C. L., Sims K. W., Perfit M. R., Blichert-Toft J. and Blusztajn J. (2011) Perspective on the genesis of E-MORB from chemical and isotopic heterogeneity at 9–10 N East Pacific Rise. *J. Petrol.* **52**(3), 565–602.
- White W. M. and Hofmann A. W. (1982) Sr and Nd isotope geochemistry of oceanic basalts and mantle evolution. *Nature* 296, 821–825. https://doi.org/10.1038/296821a0.
- White W. M., Tapia M. D. and Schilling J. G. (1979) The petrology and geochemistry of the Azores Islands. *Contrib. Miner. Petrol.* 69(3), 201–213.
- White W. M., Albarede F. and Telouk P. (2000) High-precision analysis of Pb isotope ratios by multi-collector ICP-MS. *Chem. Geol.* **167**, 257–270.
- Widom E. and Shirey S. B. (1996) Os isotope systematics in the Azores: implications for mantle plume sources. *Earth Planet.* Sci. Lett. 142(3), 451–465.
- Widom E. and Farquhar J. (2003) Oxygen isotope signatures in olivines from São Miguel (Azores) basalts: implications for crustal and mantle processes. *Chem. Geol.* **193**(3), 237–255.
- Widom E., Carlson R. W., Gill J. B. and Schmincke H. U. (1997) Th–Sr–Nd–Pb isotope and trace element evidence for the origin of the São Miguel, Azores, enriched mantle source. *Chem. Geol.* 140(1), 49–68.
- Widom E., Hoernle K. A., Shirey S. B. and Schmincke H.-U. (1999) Os isotope systematics in the Canary Islands and Madiera: lithospheric contamination and mantle plume signatures. J. Petrol. 40, 279–296.

Yu, H. (2011) Li, Hf and Os isotope systematics of Azores basalts and a new microwave digestion method for Os isotopic analysis. Doctoral dissertation, Miami University.

Zanon V., Kueppers U., Pacheco J. M. and Cruz I. (2013) Volcanism from fissure zones and the Caldeira central volcano of Faial Island, Azores archipelago: geochemical processes in multiple feeding systems. *Geol. Mag.* **150**(3), 536–555.

Zindler A. and Hart S. (1986) Chemical geodynamics. *Annu. Rev. Earth Planet. Sci.* **14**, 493–571.

Associate Editor: Julie Prytulak